AD-A083 341 MISSION RESEARCH CORP SANTA BARBARA CA F/G 20/14
EVALUATION OF AN AMBIENT HF SKY-WAVE PROPAGATION MODEL.(U)
NOV 78 W A SCHLUETER DNA001-78-C-0237
UNCLASSIFIED MRC-R-418 DNA-4780T NL

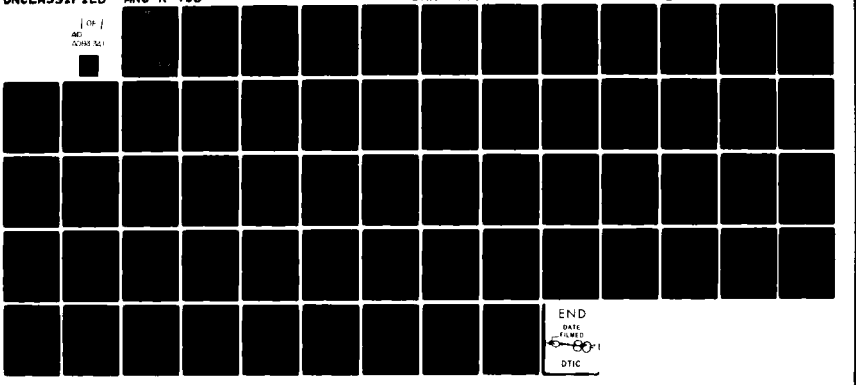

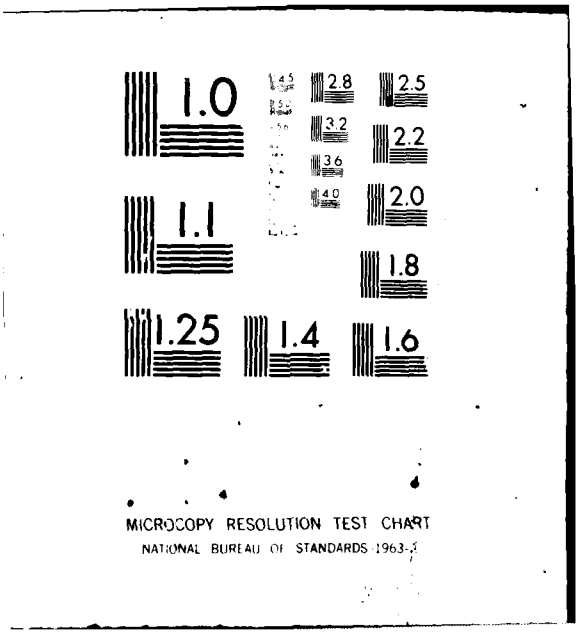
1.0
1.1
1.25
1.4
1.6
1.8
2.0
2.2
2.5
2.8
3.2
3.6
4.0
MICROCOPY RESOLUTION TEST CHART
NATIONAL BUREAU OF STANDARDS 1963-A

DNA 4780T

EVALUATION OF AN AMBIENT HF SKY-WAVE PROPAGATION MODEL

W.A. Schlueter
Mission Research Corporation
P.O. Drawer 719
Santa Barbara, California 93102

1 November 1978

Topical Report for Period 1 November 1977—31 October 1978

CONTRACT No. DNA 001-78-C-0237

THIS WORK SPONSORED BY THE DEFENSE NUCLEAR AGENCY
UNDER RDT&E RMSS CODE B322078464 S99QAXHB05309 H2590D.

Prepared for
Director
DEFENSE NUCLEAR AGENCY
Washington, D. C. 20305

Destroy this report when it is no longer needed. Do not return to sender.

PLEASE NOTIFY THE DEFENSE NUCLEAR AGENCY, ATTN: STTI, WASHINGTON, D.C. 20305, IF YOUR ADDRESS IS INCORRECT, IF YOU WISH TO BE DELETED FROM THE DISTRIBUTION LIST, OR IF THE ADDRESSEE IS NO LONGER EMPLOYED BY YOUR ORGANIZATION.

UNCLASSIFIED

SECURITY CLASSIFICATION OF THIS PAGE *(When Data Entered)*

REPORT DOCUMENTATION PAGE		READ INSTRUCTIONS BEFORE COMPLETING FORM
1. REPORT NUMBER DNA 4780T	2. GOVT ACCESSION NO. AD-A083341	3. RECIPIENT'S CATALOG NUMBER
4. TITLE *(and Subtitle)* EVALUATION OF AN AMBIENT HF SKY-WAVE PROPAGATION MODEL		5. TYPE OF REPORT & PERIOD COVERED Topical Report for Period 1 Nov 1977 - 31 Oct 1978
		6. PERFORMING ORG. REPORT NUMBER MRC-R-418
7. AUTHOR(s) W. A. Schlueter		8. CONTRACT OR GRANT NUMBER(s) DNA 001-78-C-0237
9. PERFORMING ORGANIZATION NAME AND ADDRESS Mission Research Corporation P.O. Drawer 719 Santa Barbara, California 93102		10. PROGRAM ELEMENT, PROJECT, TASK AREA & WORK UNIT NUMBERS Subtask S99QAXHB053-09
11. CONTROLLING OFFICE NAME AND ADDRESS Director Defense Nuclear Agency Washington, D.C. 20305		12. REPORT DATE 1 November 1978
		13. NUMBER OF PAGES 62
14. MONITORING AGENCY NAME & ADDRESS*(if different from Controlling Office)*		15. SECURITY CLASS *(of this report)* UNCLASSIFIED
		15a. DECLASSIFICATION DOWNGRADING SCHEDULE

16. DISTRIBUTION STATEMENT *(of this Report)*

Approved for public release; distribution unlimited.

17. DISTRIBUTION STATEMENT *(of the abstract entered in Block 20, if different from Report)*

18. SUPPLEMENTARY NOTES

This work sponsored by the Defense Nuclear Agency under RDT&E RMSS Code B322078464 S99QAXHB05309 H2590D.

19. KEY WORDS *(Continue on reverse side if necessary and identify by block number)*

HF Propagation
Ionospheric Models
HFNET

20. ABSTRACT *(Continue on reverse side if necessary and identify by block number)*

The ambient sky-wave propagation model in the HFNET computer program is evaluated by comparing predicted results with those from the widely used HFMUFES4 computer program and data from mid-latitude and auroral region propagation paths. The HFNET propagation model consists of two parts—a geometrical model and an ionospheric parameter model.

The HFNET geometrical model uses the virtual height technique with corrections made for ionospheric tilts in and perpendicular to the great circle

DD FORM 1 JAN 73 1473 EDITION OF 1 NOV 65 IS OBSOLETE

UNCLASSIFIED

SECURITY CLASSIFICATION OF THIS PAGE *(When Data Entered)*

20. ABSTRACT (Continued)

plane. Good agreement between results from HFNET and HFMUFES4 was obtained when the same ionospheric parameters (for a horizontally uniform ionosphere) were used in both programs. Comparison of program results with data from a 3,260 km mid-latitude propagation path showed good agreement, thereby establishing the validity of the geometrical model.

HFNET predictions were seen to depend upon models of ionospheric parameters. This dependence, of course, applies to all models of sky-wave propagation. HFNET allows the user to select one of two ionospheric models of median characteristics. One model is global in nature while the second model applies only to latitudes greater than about 45°. Comparison of HFNET results using the global model with data from the mid-latitude path shows that the predicted MUF is 5 percent to 20 percent below the average of daily values obtained over a month's time. However, the HFNET values are within the wide range of observed daily variability. For frequencies below the MUF, those generally used so as to avoid the problems associated with operating near the highly variable MUF, predicted and measured characteristics such as elevation angle and mode type are in good agreement. For the case of auroral region propagation, good agreement between predicted and measured values of MUF were obtained.

HFNET calculates the deviation of azimuthal arrival angle from the great-circle direction which is caused by ionospheric tilts. Predicted values are substantially smaller than those measured, but this is thought to arise from the use of median ionospheric parameters. That is, small spatial variations in ionospheric parameters are eliminated in the process of reducing large quantities of measured ionospheric data to models of average characteristics.

PREFACE

I would like to thank Dr. D. H. Sowle for many helpful discussions regarding the ambient HF sky-wave models. Mark Frolli and Jim Speer of MRC provided considerable help in incorporating the auroral region ionosphere model into HFNET and in analyzing the program's output.

I am also pleased to acknowledge the cooperation and assistance extended by Dr. T. J. Elkins and his group at Rome Air Development Center, Hanscom Field, Massachusetts in providing their ionospheric model and answering questions concerning its operation.

CONTENTS

ILLUSTRATIONS

TABLES

SECTION 1
INTRODUCTION

This report evaluates models of HF ambient sky-wave propagation used in the HFNET computer program. HFNET has been under development since 1975 and, at present, represents an advanced capability in predicting HF and VHF propagation in a nuclear burst environment. Improvements to the program implemented during FY78 included an improved ionospheric model for the auroral region, improved nuclear burst phenomenology, and the addition of nuclear burst produced propagation paths at HF and VHF frequencies (bomb modes).

In the evaluation of the ambient propagation models, the question arises as to what data or information is to be used as the standard or bench mark again which HFNET results are to be compared. Very little measured data on ambient sky-wave propagation is available in the technical literature. However, a report on a link from Slough, England to Cypress contains data in a form for use in the evaluation of the equatorial and mid-latitude ionospheric model. Another report summarizes data on auroral links from Caribou, Maine to stations in Greenland and Iceland and is used in an evaluation of auroral propagation models. Whenever applicable, within non-auroral regions, comparisons of HFNET with HFMUFES4, an extensively used equatorial and mid-latitude ambient HF propagation program, will be made.

Section 2 will describe the ambient propagation models used in HFNET and the two ionospheric models. Section 3 will compare predicted values from HFNET with data and HFMUFES4 predictions. Section 4 will

present conclusions drawn from this study. An appendix contains examples of predictions for hypothetical mid-latitude paths of 2,000 km and 4,000 km.

SECTION 2
AMBIENT MODE CALCULATIONS

2.1 HFNET PROGRAM DEVELOPMENT

The HFNET computer program has been developed by MRC under DNA sponsorship to study sky-wave propagation in a nuclear burst environment, with particular emphasis on the evaluation of many communication links subjected to the effects of a large nuclear burst scenario. A brief review of the history of its development to its present form will show the philosophy of design improvements and application to technical problems of specific interest to DNA.

The HFNET program was originally developed for application to studies of the late time reconstitution of HF communications within CONUS following the high altitude portion of the NICKEL PLATE scenario. For that application, a much simplified model of late-time, nuclear burst absorption effects was developed in order to achieve decreased code running time with little (if any) loss in computational accuracy. In that version, the HF sky-wave parameters were generated externally to HFNET using the HFMUFES4 computer program developed by ITS for general studies of sky-wave propagation[1]. An evaluation of HFNET was made by comparing its predicted values to measured values of propagation from the 1962 U. S. nuclear test series.

At that time, it was recognized that it was necessary to improve the predictions of sky-wave propagation beyond that used in the HFMUFES4 program. HFMUFES4 was developed for very general studies of sky-

wave propagation and was not intended to be used in very detailed evaluations such as those of interest to DNA. Thus, MRC developed a more detailed calculational model[2] of propagation to be included within HFNET which would include ionospheric tilts, both in and perpendicular to the great-circle plane, produced by ambient electron density gradients. Since this model was constrained to be fast running, the virtual height technique of calculating sky-wave reflection altitudes, as used in HFMUFES4, was used along with a fast-running, analytic model of the global ionosphere[3,4]. The program in this form was applied to a DNA-sponsored analysis of the Cemetery Net communication system performance in a nuclear burst environment.

During 1977, MRC began an evaluation of the proposed ITT adaptive HF/VHF communication system with the initial emphasis on developing the methodology for evaluating the system and examining the propagation models which would be required for these studies. Major improvements to HFNET were proposed for these studies, including the use of an auroral region ionosphere, models of HF and VHF anomalous propagation from striated regions produced by high altitude nuclear bursts (so-called "bomb" modes), and other non-median ionospheric effects. These improvements have been introduced into HFNET during FY78, and initial evaluations of the ITT system are underway.

Bearing in mind that HFNET is designed to evaluate HF system performance in a nuclear burst environment, the rationale for the ambient propagation model is best stated in the following quotation from Reference 2.

> "Anticipated nuclear effects which may conveniently be taken into account by alteration of normal ionospheric parameters are changes in ambient layer (i.e., F_2, F_1, or E-layer) electron density, thickness, height, and tilt due to (1) propagation of acoustic gravity waves, (2) ducted waves, (3) burst region disturbance (F-layer depletion, etc.), or (4) bomb or

debris irradiation. Another set of effects exists (M-modes, fireball modes, plume modes, etc.) which are more conveniently calculated independently and which will not concern us here. To calculate, even crudely, effects of the above list on propagation geometry, thus on existence and efficiency of ambient-like modes and creation of new modes, the ambient mode calculation must readily take into account ionospheric variations all along the propagation path in terms of variability of reflection height and ionospheric tilt, both along and across the great-circle path. In fact, non-great-circle propagation must be treated. The current ITS78 code, the community standard, evaluates ionospheric conditions only at the great-circle path center, derives from that a single reflection height and does not consider tilt or off-great-circle propagation. This is satisfactory for long-term, average predictions, the objective of that code, but does not lend itself to situations similar to nuclear effects where a portion of the path is strongly disturbed....

"The method developed here to meet requirements of nuclear effects studies is approximate but more accurate than justified by predictability of either the ambient or nuclear disturbed ionosphere. It is more expensive in computer time than one would prefer but still vastly cheaper than normal ray trace techniques; sophisticated in that it accounts for ionospheric variation, tilt, and off-great-circle propagation; but in its present implementation rudimentary in that only two modes can be calculated for a given number of hops, no extraordinary ray modes are calculated, etc. The restriction to two modes per hop number could be readily remedied and this, at least, is hoped to be done soon. The basic technique is believed to be feasible. As reported here, the method has been developed to a useful state, one that is more realistic than others in many important respects, as well as one that is reasonably inexpensive in application."

2.2 GEOMETRICAL MODE CALCULATIONS

The model of HF sky-wave modes is described in detail in Reference 2 and is not expected to be changed in any future

computer program revision. Although recent versions of HFNET include an auroral ionosphere model, the mode calculations have not changed. A brief outline of the model, extracted from Reference 2, is contained below.

Mode geometry is specified in terms of the ends of a number of straight line segments (passes) connecting reflection points. A one-hop mode is specified by latitude, longitude, and altitude above the earth's surface of three-line segment ends: (1) the transmitter coordinates; (2) the equivalent triangular ionospheric reflection point; and (3) the receiver coordinates. A two-hop mode requires specifications of coordinates for five points—the two end points, two ionospheric reflection points, and an intermediate surface reflection point. In general, three space coordinates must be specified for $2n + 1$ points for an n-hop mode.

A mode fails to exist if (1) the F_2 layer fails to reflect the ray on any hop; (2) transmitted launch angle for the mode is below a specified value; (3) received angle is below a specified value; (4) ionospheric tilt causes the ray to be reflected back upon itself; or (5) ionospheric tilt causes the ray to be deflected forward at too great an angle.

Steps in calculation of n-hop mode geometry are as follows:

1. The great-circle path is divided into n equal segments, one for each hop.
2. For each segment, a one-hop mode is calculated according to local ionospheric conditions as follows:
    a. Assume reflection occurs at the F_2 layer; calculate the equivalent triangular reflection altitude, h_r, for a parabolic layer by iteration.

b. If successful, calculate refraction effect due to the F_1 layer. If the F_1 layer reflects the ray, carry out step *a* for the F_1 layer.

c. Calculate refraction effect due to the E-layer. If the E-layer reflects the ray, carry out step *a* for the E-layer.

At the completion of step 2, the situation is depicted in the sketch, provided all hops were successfully reflected.

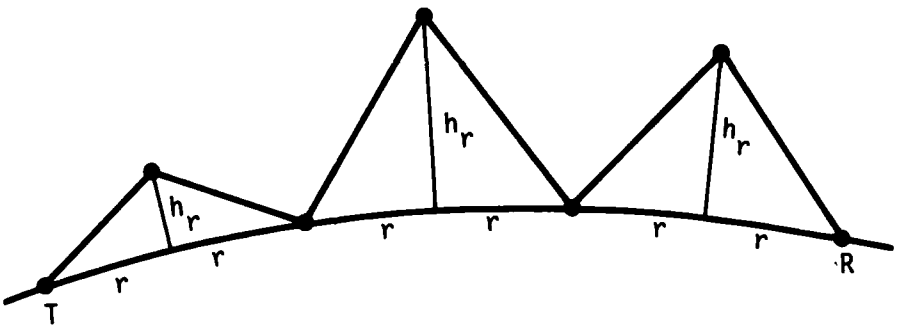

At this point, the mode is specified by the latitude and longitude of the end points. These are equally spaced along the great-circle path but each ionospheric reflection height is different, a violation of the laws of optics.

3. Adjust the pass ranges r_i, so that incident and reflected angles are equal, accounting for differences in h_r.

4. Calculate ionospheric tilt angles both along the great-circle and across the great-circle at each ionospheric reflection point.

5. Adjust all pass coordinates (latitude, longitude, altitude) to account for tilt along the great-circle to first order in tilt angle (that is, in the vicinity of each reflection point, the tilt is constant). If the ray is reflected back upon itself at any point, or if the cumulative effect of all tilts causes the ray to land too far beyond the receiver, reject the mode.

6. Calculate off-great-circle displacements of all pass coordinates and new reflection altitudes due to across-great-circle tilt.

7. Find launch and received ray elevation angle relative to the horizon, and azimuth relative to the great-circle path. If either elevation is below a specified limit, reject the mode.

At the end of this process an approximation has been found to a "good" propagation mode with specified number of hops, within the limitations indicated above. The sketch below illustrates the situation in the great-circle plane at the end of the calculation.

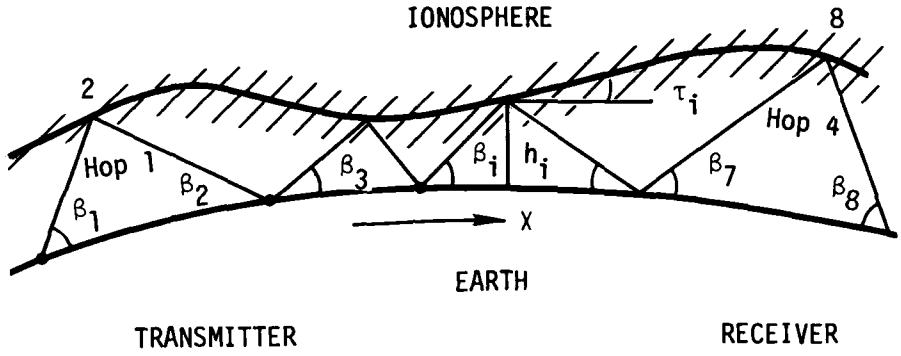

Note that the only iterations occur in finding single-hop solutions to reflection from a single parabolic layer in Step 2. With this exception, the mathematical treatment runs "open loop" and could be made more rigorous by iterating on each refraction correction, after range correction for differing reflection heights, and after corrections for tilt. Such a procedure would be prohibitively expensive in calculation time and would produce numerical results significantly different from the present technique only for cases where some reflection occurred very near a critical point (e.g., almost or barely reflected off some layer). Predictability of either natural or disturbed ionospheric conditions is not sufficiently accurate to justify such fine tuning.

Of much greater importance is the fact that this method does not calculate all possible "sensible" rays. This defect is illustrated in the next sketch, done in plane geometry for illustrative purposes.

This technique first finds a tentative (low or Pederson) ray which reflects off the highest available layer (the dashed ray of the sketch which reflects in the vicinity of point A). Next the refraction angle due to passage through the lower layer at point B is calculated.

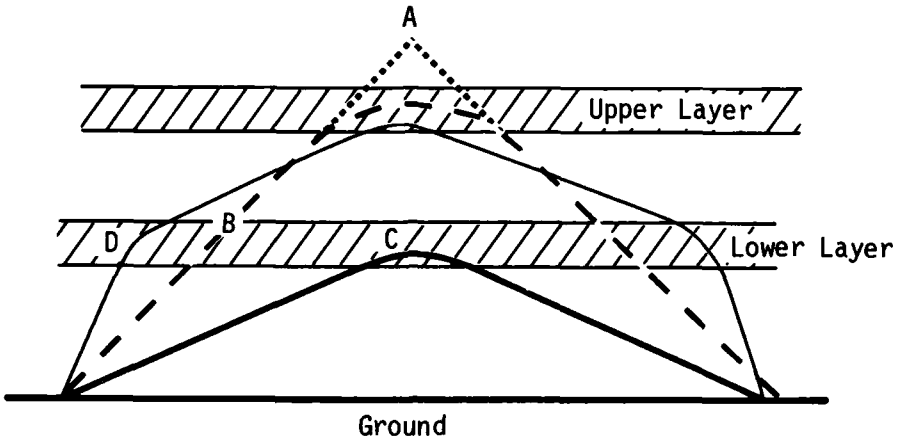

If refraction is not large enough to reflect the ray at B, a correction to the effective triangular reflection point A is introduced and the calculation proceeds to the next step. At this point, our technique has irretrievably missed a potential lower ray which reflects at C. Under almost all ambient conditions, the lowest ray suffers greater absorption and also is a more likely candidate for rejection due to low launch angle; thus, is not likely to be useful or to cause multipath problems. It is unusual, but possible, that nuclear effects could preferentially interfere with the upper ray enough to make the ray at C the best mode.

2.3 COMPARISON OF CALCULATIONAL TECHNIQUE WITH HFMUFES4

Much of the HFNET ambient propagation formulation is similar to that used in HFMUFES4. The virtual height model along with refractive effects arising from a lower layer are identical in both cases. However, HFMUFES4 evaluates ionospheric conditions at the great-circle path center thereby using a uniform (horizontally) ionosphere. There is no consideration of tilt in the great-circle or non-great-circle planes. This model is satisfactory for long-term, average predictions—the object of the HFMUFES4 program.

2.4 IONOSPHERIC MODELS

The ionospheric model creates a data table of ionospheric parameters for each desired transmitter-receiver link. Each such data table consists of three sets (one for each ionospheric layer, E, F_1, F_2) of three parameters describing parabolic ionospheric layers above several points on the great-circle path at a number of times. The three-layer parameters are (1) maximum electron density; (2) thickness of the layer; and (3) altitude of the maximum electron density. The spatial points are arbitrary in number and spaced equally along the great-circle path. The number of times is also arbitrary and determines the number of equal segments of a 24-hour period at which each layer will be specified at each point along the great-circle. Normally, 24 times are chosen, one for each hour of the day (plus one repeated entry to allow the table to begin at 0 hours and end at 24 hours), and seven space points, which yield six equally spaced points along the path (both end points are included). Normally, these great-circle points are separated by less than 15° of arc each (that is, corresponding to less than an hour apart local time). With ionospheric models at our disposal, one hour equivalent segments have been found to be about twice as dense as necessary to allow interpolation in both space and time to the limit of model fidelity.

The purpose of this array is to allow rapid interpolation in space and time for ionospheric quantities without having to repeatedly apply potentially complex ionospheric models for identical or similar conditions. Heights and thickness are interpolated linearly and electron density logarithmically between adjacent points.

2.4.1 Equatorial and Mid-Latitude Ionospheric Model

Y. T. Chiu of the Aerospace Corporation has developed a phenomenological model of ionospheric electron density on a global basis, with specific dependence on diurnal, annual, and solar activity cycles[4].

The model is constructed from monthly-averaged, hourly ionospheric sounding data from about 50 stations during the epoch 1957-1970, as provided by the World Data Center, Boulder, Colorado. The basic premise of the model is that the average electron density at any point in space, time, and solar condition is the sum of contributions from each of three layers whose electron density is the product of a global amplitude constant, a vertical profile function, and a layer peak density function. The profile functions are of the standard Chapman forms while the layer peak density function contains the greater part of the space-time variation. In HFNET, an approximate analytic expression is used to convert the characteristic form of the Chapman layer below the peak electron density to the parabolic form used in the propagation model.

The ionospheric sounding data from the World Data Center, used by Chiu in formulating his model, is also the data base from which world-wide maps of ionospheric parameters are derived for use in HFMUFES4 (Reference 1). However, in this latter case, a two-layer ionosphere was formulated.

Figure 1 shows a typical comparison of the three-layer parabolic approximation used in HFNET with the Aerospace model, the two-layer HFMUFES4 model, and with data taken at Arecibo, Puerto Rico. Cases can readily be found resulting in better and worse agreement with data. The figure illustrates a general result, appearing to be valid for all ionospheric models which might be used as a basis for the fit: The error resulting from the three parabolic layer approximation is small compared with the error due to daily fluctuations of the real ionosphere. In Section 3, the variation in predictions of propagation due to uncertainties in ionospheric parameters will be discussed in detail.

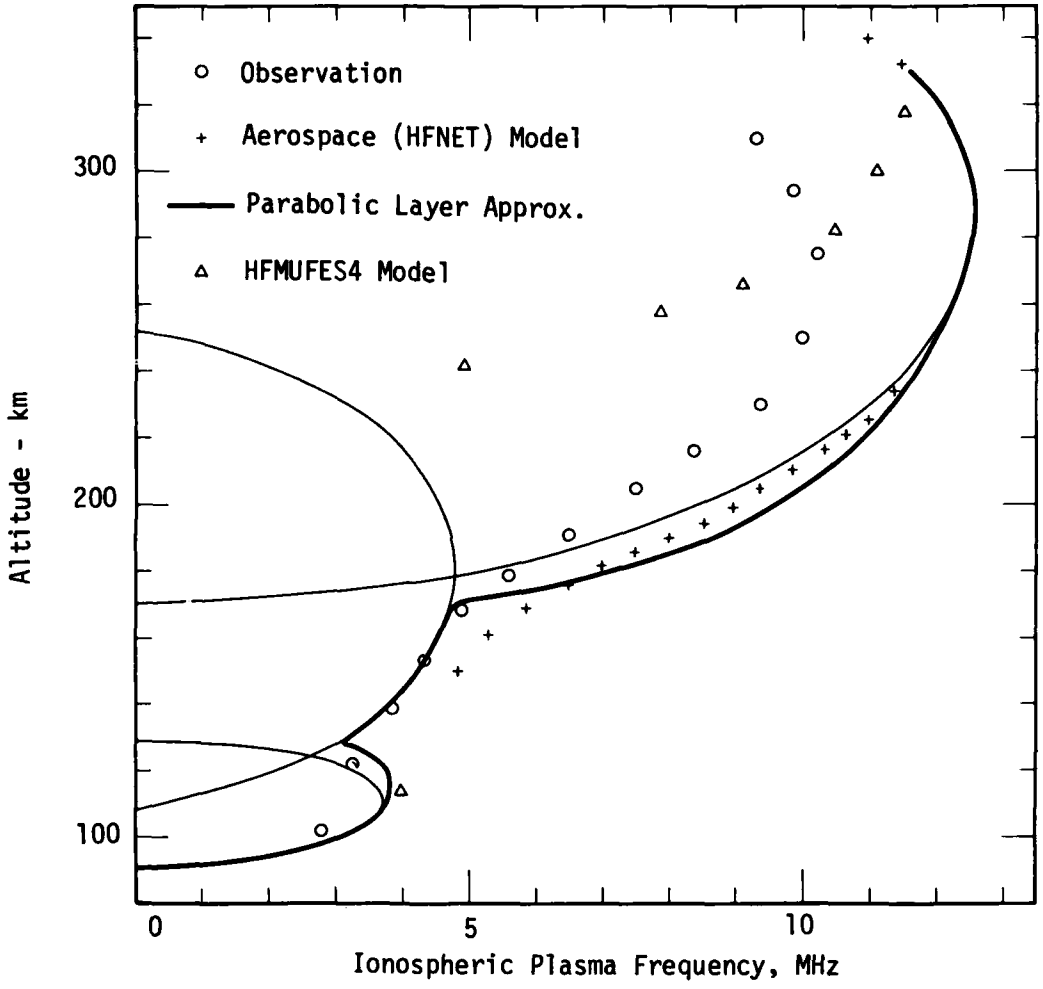

Figure 1. Typical ambient ionosphere—Arecibo, Puerto Rico; local time = 1200; smoothed Zurich sunspot number = 110..

2.4.2 Polar Ionospheric Model

An empirical model of the polar ionosphere has been developed by the Rome Air Development Center[5] (RADC) and modified by Stanford Research

Institute[6] (SRI). The main features of this model, which will hereafter be called the RADC model, will be described next.

Quoting from Reference 5, the RADC model "is intended primarily to provide the information necessary to plan and implement systems, operating or planned to operate in the polar environment which make use of radio waves propagated either via or through the ionosphere.... The present model is largely empirical, since the complexity of the physical processes in the polar ionosphere makes an accurate theoretical model impossible at present."

The data base of ionospheric parameters is the result of routine sounding measurements from 45 stations most of which are located at latitudes greater than 40° N. The model is, therefore, limited to applications for latitudes above this value.

A distinguishing feature of the polar ionosphere is the treatment of effects produced by solar particles. Electrons and protons are included in the solar wind which interacts in a complex manner with the earth's magnetic field, resulting in energy deposition from low altitudes characteristic of the D-region (∿40 km) to high altitudes at the top side of the F-layer. The polar region ionospheric effects are generally restricted to the auroral oval region which roughly corresponds with the ionospheric projection of the boundary between open and closed field lines in the magnetosphere. The oval remains fixed with respect to the sun while the earth rotates beneath it. Because of the angle between the earth's magnetic and spin axes, a complex variation of magnetospheric particle precipitation results, when viewed from a single geographic position.

The effect of varying solar particle radiation is accounted for in the RADC model through dependence of ionospheric parameters on the K_p geomagnetic activity index[7].

The K_p index, a quasi-logarithmic scale ranging from 0 to 9, is a 3-hour index of world-wide geomagnetic activity derived from the weighted records of 12 standard magnetic observatories. At each station, the three-hour range index, K, is derived from local three component magnetometer measurements for three-hour intervals of universal time. For each time interval, the maximum deviation, δmax, of the three components of magnetic field is recorded, and it is on this measurement that K is based. Each observatory has its own table for converting δmax to the quasi-logarithmic index K, the values in the table being determined by the geomagnetic latitude of the observatory. Values of K range from 0 (low activity) to 9 (strong activity); the ratio of δmax at strong activity to low activity is a factor of 100.

Before the world-wide activity index K_p is derived, the local K values are converted to quasi-logarithmic K_s values, running through 28 values, from 0 to 9 in steps of 1/3, depending upon local time, position, and season. This intermediate conversion from K to K_s provides for local diurnal and seasonal variations in geomagnetic activity. The planetary index K_p is an average of the K_s indices from the participating observatories. The steps of 1/3 in K_p values are indicated by superscript + or -. Thus, values of 2 1/3 and 2 2/3 are denoted by 2^+ and 3^-, respectively.

Although the RADC polar ionosphere model accepts a planetary K_p value as input and as a convenience to the user, this K_p value is converted to a local K value depending upon position, time, and season. The local K value is used to scale ionosphere characterisitcs since it was found that this local characterization of geomagnetic activity gave a much better correlation among the various ionospheric sounding data than did the world-wide index.

The characteristics of the various regions of the ionosphere will be described briefly in order to indicate the dependence of various

features on the type of solar radiation. It is important to realize that, although the response of the ionosphere to solar radiation is generally understood, detailed models which correlate incident solar radiation with specific ionospheric characteristics are not available.

2.4.2.1 E-Region. The E-region spans the altitude range from about 85 km to 140 km. Ionization arises from two separate processes—X rays and, in the polar region, particle deposition. The contribution from solar X rays depends upon solar zenith angle, χ, according to a law of the form $N \sim (\cos \chi)^n$. The parameter n ranges from 0.6 to 0.8, depending on seasonal and latitudinal factors. The contribution from X rays does not drop to zero at night because of atmospheric scattering of solar X rays from the daytime to nighttime portion of the atmosphere.

The RADC polar model includes contributions to E-layer ionization from deposition of charged particles. This contribution is coupled to the K_p index and is, of course, independent of the effect of solar X rays. The auroral E-layer varies with magnetic activity, magnetic time, and magnetic latitude. It resembles the X ray produced E-layer but occurs on both day and night sides of the earth. It is different than the sporadic E-layer (to be described next) by varying more slowly in space and time, and being much thicker. However, as in the case of sporadic-E, the auroral E-layer characteristics are essentially random variables.

Sporadic E (E_s) refers to regions of highly enhanced electron density, often thin and patchy, causing abrupt, mirror-like reflection of radio waves. These effects are observed at all latitudes, although the physical origin within equatorial, mid-latitude, and auroral regions is generally thought to be different. Equatorial E_s arises from irregularities produced by the unstable plasma of the electrojet. At mid-latitudes, it is formed by natural wind induced compression of metallic ions resulting

from meteoric ablation in the lower E-region. Within the auroral region, it is produced by highly variable (in space and time) deposition of charged particles. Examination of ionospheric sounder data indicates that median lifetimes of E_s are of the order of three to four minutes and that typical dimensions are of the order of 3 to 4 $\times$ 10^5 km^2. There is a high correlation between E_s and visible auroral features, and this correlation is the basis for the assumption that the morphology of E_s is similar to the visible aurora. Thus, E_s is characterized by the auroral oval and is assumed to occur, on the average, continuously around the oval.

The RADC model sums the contribution to the E-layer from individual components, i.e., solar X rays, auroral particles, and sporadic E.

2.4.2.2. F-Region. The F-region extends from about 140 to several thousand kilometers. Soft solar X rays ionize the atmosphere in this region. The lower F-region below about 200 km, known as the F_1-layer, behaves very differently from the upper (F_2) region. In the F_1-layer, where molecular ions predominate, the electron recombination rate is high, and the ionization density follows a solar zenith angle dependence similar to that of solar X rays produced in the E-region.

In the polar region, the F_1-layer shows an anomaly in that this layer does not appear during winter months, despite the fact that the solar zenith angle dependence shown earlier would indicate its existence whenever the sun is above the horizon. One possible explanation is a seasonal dependence of the composition of the neutral atmosphere which gives rise to changes in the electron loss coefficients at F_1-layer heights.

The F_2-layer is the upper portion of the F-region where atomic species predominate. Slower recombination occurs than in the F_1-layer

so that electron density values are determined primarily by diffusion and convection, rather than by photochemistry.

A special feature of the polar ionosphere is the high latitude trough which is a depression in the altitude of the peak electron density in the F_2-layer in going from mid-latitude to high latitude values. The trough is a complex feature whose location roughly coincides with the ionospheric projection of the plasmapause. Although the physical processes which produce the trough are not fully understood, it is thought to be due to a combination of effects from the solar wind, auroral particle precipitation, and thermal conduction from the magnetosphere.

Spread F is the term applied to certain observed behavior of the F-layer. It is often found that the duration of return of an ionospheric sounder signal is much longer than the duration of the incident pulse; hence, it is described as a spread-F echo. The spread of the echo is associated with scattering in the F-layer caused by fluctuations in ambient electron density. The physical basis for these fluctuations is complex and not fully understood. Furthermore, as in the case of sporadic E, the physical mechanism for its generation varies considerably with latitude.

The RADC model does not include spread-F effects. However, recent studies of the scintillation of transionospheric radio wave propagation at VHF and higher frequencies[8,9] have resulted in a global model of F-layer electron density variations. This non-RADC model is used as the model of electron density variations giving rise to spread-F effects.

2.4.2.3. Auroral D-Region Absorption. The D-region is the lowest portion of the ionosphere extending from about 40 km to 85 km. The principal sources of ionization are solar hydrogen Lyman alpha radiation, hard X rays, and—at lowest altitudes—galactic and solar cosmic rays.

Negative ions are important in D-region chemical reactions whereas they are insignificant at high altitudes. The D-region electron density undergoes a pronounced diurnal variation, with rapid recombination and attachment to neutral molecules taking place after sunset. The high neutral species density results in high electron collision frequencies in this altitude range leading to absorption of radio waves passing through it.

At equatorial and mid-latitudes, ambient electron densities in the D-region are essentially controlled by solar illumination. Models of radio wave attenuation at these latitudes can be predicted by nominal values of predicted ambient electron densities. However, at high latitudes, there is a strong dependence of D-region electron densities on magnetic substorm activity and the resultant deposition of charged particles. A model of auroral D-region absorption dependence on K_p has been developed[6] and is included in the RADC model.

SECTION 3
RESULTS

This section will discuss predictions from several computer programs as well as experimental data from a variety of sources. First, results will be described from a study of the effect of naturally occurring ionospheric variability upon predictions of propagation characteristics for hypothetical paths. Then, in separate discussions of mid-latitude and auroral regions, comparison of HFNET and HFMUFES4 predictions with measured propagation characteristics will be made. The characteristics to be compared include the mode type, elevation and azimuthal arrival angles, and maximum propagation frequency.

One parameter which is convenient to compare is the maximum frequency which propagates between a transmitter and receiver at an instant in time; however, there is an inconsistency in nomenclature among all of the data sources (experimental and predictive). Regarding the acronyms MUF and MOF, the following usage will be made. MUF (maximum usable frequency) will refer to predictions of the maximum propagating frequency, and MOF (maximum observed frequency) will refer to experimentally measured values of the maximum propagating frequency. In this sense, the terms MOF and MUF can be considered interchangeable. A potential source of confusion in usage within this report is the consideration of HFMUFES4 results because, in that program, the MUF is defined as the propagating frequency with the probability of occurrence equal to 0.50. HFMUFES4 calculates other modes with frequencies greater than the MUF but with lower probability. We will try to clarify the usage of terminology when necessary.

3.1 DAILY VARIABILITY OF THE IONOSPHERE

The results of a comprehensive study of the variability of the ionosphere and its effect on HF radio propagation will be discussed in some detail to illustrate this important process which, it will be seen, has an important influence in the study of HFNET propagation modeling. Reference 10 describes work in which models of the variability of two important F-layer parameters—F_2 layer critical frequency, f_oF_2, and altitude of the peak F_2-layer electron density, h_mF_2—were derived for use in a three-dimensional ray tracing computer program. From the ray tracing program, values of the maximum usable frequency (MUF) were obtained for hypothetical paths of 2,000, 2,500, and 3,000 km and for median and non-median ionospheric parameters.

In this work, the use of median values of E-layer characteristics was justified from the fact that the standard deviation of E-region critical frequency, f_oE, about its monthly median is of the order of 5 percent—the E-layer is comparatively stable. The standard deviation of f_oE is about two to five times smaller than that of f_oF_2.

Relative deviations during 1966 of f_oF_2 and h_mF_2 were derived from 10 stations between 30° and 70° N. latitude where the density of observations and data lead to the smallest uncertainty in reconstruction of ionospheric behavior. It was seen that standard variations in h_mF_2 ranged from 5 percent to 10 percent whereas variations in f_oF_2 were about 20 percent at night and 10 percent during daytime. It should be recalled that the electron density is related to critical frequency as

$$N_e = 1.24 \times 10^4 \, f^2 \qquad (cm^{-3})$$

for the critical frequency f in MHz. Thus, electron density, the parameter of interest, is proportional to critical frequency squared, and

variability in critical frequency has a pronounced effect on electron density variability. For example, typical values of f_oF_2 range between 4 MHz and 9 MHz. Table 1 lists values of electron density at various critical frequencies. It is seen that a ± 25 percent variation in a 4 MHz critical frequency; namely, ± 1 MHz, corresponds to a range of electron density of about 1×10^5. The same relative variation at 9 MHz, ± 2.25 MHz, produces an electron density variation of about 5×10^5.

Table 1. Electron density at several critical frequencies.

Critical Frequency (MHz)	Electron Density (cm^{-3})
3	1.1×10^5
4	2.0×10^5
5	3.1×10^5
6.75	5.6×10^5
9	1.0×10^6
11.25	1.56×10^6

The changes in MUF at three times and for three ranges are listed in Table 2 (from Reference 10).

Similar results were obtained by simultaneous variation in f_oF_2 and h_mF_2. That is, when the change in one parameter is such as to increase (decrease) the MUF, and the change in the other is to increase (decrease) the MUF, the combined effect is an even further increase (decrease). Similarly, if one parameter increases the MUF while the other decreases it, the effect of the combined change is for the MUF to fall between the two extremes.

Table 2. Changes in MUF produced by daily ionospheric variability.

GMT (hr)	0000	0600	1200
2000 km range			
Median MUF	10.5 MHz	13.0 MHz	20.5 MHz
Med + F_2+*	12.5(+19)**	17.0(+31)	22.0(+7)
Med + F_2-	8.5(-19)	11.5(-12)	18.2(-11)
Med + HM +	10.0(-5)	12.5(-4)	18.5(-11)
Med + HM -	11.5(+10)	15.0(+16)	22.5(+10)
2500 km range			
Median MUF	12.0	16.5	23.0
Med + F_2+	14.5(+21)	19.0(+15)	25.5(+6)
Med + F_2-	9.5(-21)	14.0(-15)	21.5(-6)
Med + HM +	11.5(-4)	15.5(-6)	22.0(-4)
Med + HM -	13.0(+8)	18.0(+9)	26.0(+13)
3000 km range			
Median MUF	14.0	18.5	25.5
Med + F_2+	16.0(+14)	22.0(+19)	27.0(+6)
Med + F_2-	11.0(-21)	16.0(-14)	23.8(-6)
Med + HM +	13.0(-7)	18.0(-3)	24.0(-6)
Med + HM -	14.5(+4)	21.0(+14)	27.5(+8)

* The notation Median + F_2+ (Median + F_2-) refers to results derived using ionospheric structure obtained by increasing (decreasing) the median value of f_0F_2 by one standard deviation while h_mF_2 remained unchanged. Similar notation is used to identify changes in h_mF_2 while f_0F_2 is held constant.

** Values in parenthesis are percentage change from the median.

Reference 10 also presents results of the variations in elevation angle due to variations in ionospheric parameters. Typical variations in elevation angle of about 20 percent to 40 percent are reported for frequencies near the MUF.

The conclusion drawn from Reference 10 is that HF propagation programs using median data bases can yield values of MUF of the order of 20 percent to 30 percent different than measured daily values because of normal daily variability of the ionosphere. This effect will be seen in the next section which discusses observed data for the Slough, England to Cypress communication link.

3.2 RESULTS AT EQUATORIAL AND MID-LATITUDES

3.2.1 Mode Characteristics

Reference 11 reports measurements over the 3260 km path from Akrotiri, Cypress to Slough, England for 12 months during 1968-1969 at sunspot maximum. Figure 2, taken from that reference, shows daily variation in hourly values of the MUF which is consistent with the previous discussion of variations in ionospheric parameters. Monthly median values derived from the data are also shown in Figure 2; this curve is also shown in Figure 3 along with values of MUF derived from HFNET and HFMUFES4 for this link. It is seen that there is much better agreement between the monthly averaged data and HFMUFES4 predictions than between monthly averaged data and HFNET predictions except near UT = 12 hours.

In order to examine the discrepancy between measurements and HFNET predictions, a special version of HFNET was prepared which allowed use of the HFMUFES4 ionosphere. When HFNET was exercised with the HFMUFES4 ionosphere, at times of 2 hours and 10 hours, predicted values of MUF were 17.5 MHz and 24 MHz—essentially identical to the HFMUFES4 predicted values.

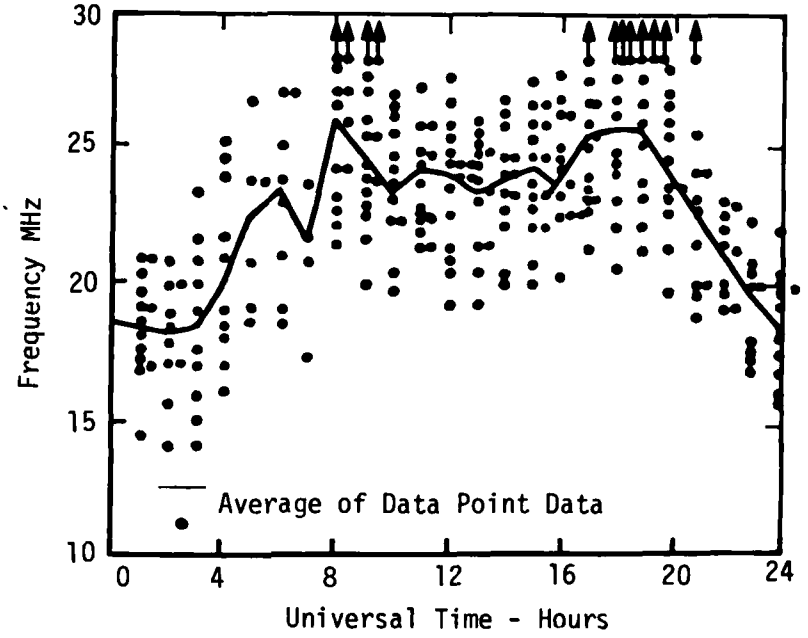

Figure 2. Maximum observed frequencies for Slough-Cypress path in July 1969.

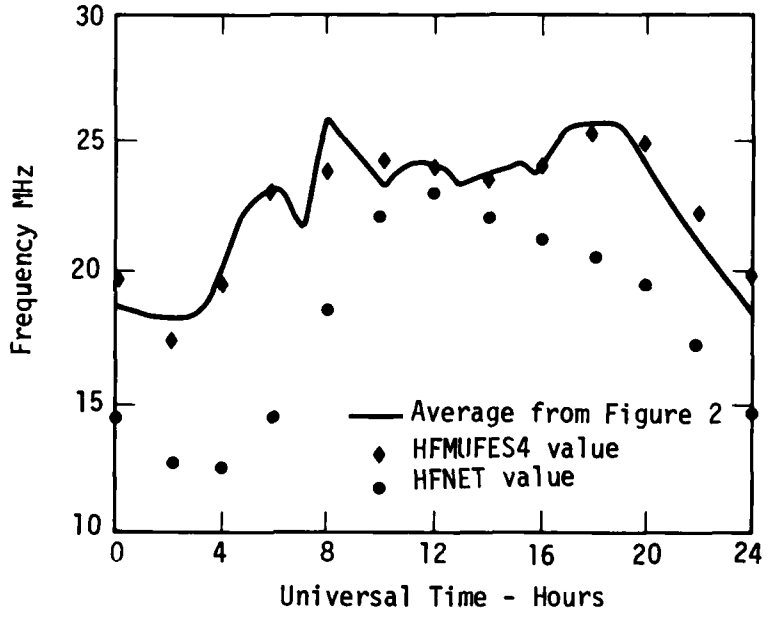

Figure 3. Comparison of average measured MUF values with those predicted by HFMUFES4 and HFNET.

Thus, the HFNET discrepancy is due to the Aerospace ionospheric model. Table 3 lists values of ionospheric parameters at the midpoint of the Slough to Cypress link at two universal times (2 hours and 10 hours). The characteristics at this position determine the one-F-hop which is essentially the MUF.

Table 3. Ionospheric parameters at midpoint of Slough-Cypress link.

	(a) UT = 2 Hours		(b) UT = 10 Hours	
	HFMUFES4	Aerospace	HFMUFES4	Aerospace
f_oE	0.99 MHz	1.01 MHz	3.68 MHz	3.71 MHz
f_oF_1	0.00 MHz	0.81 MHz	0.00	5.15 MHz
h_mF_1	-	180.00 km	-	180.00 km
f_oF_2	6.16 MHz	4.37 MHz	8.29 MHz	6.99 MHz
h_mF_2	365.90 km	345.50 km	345.90 km	302.60 km

Table 3 shows that at UT = 2, the Aerospace f_oF_2 is about 70 percent of the HFMUFES4 value. Since the electron density is proportional to frequency-squared, the Aerospace electron density is only one-half that of HMUFES4. At 10 hours time, the difference between model critical frequencies is substantially less, giving rise to better agreement between predicted values.

While the preceding discussion has been oriented toward comparing predicted and measured values of MUF, recall that this parameter is selected only as a convenience. Of higher importance for calculations of communication system's performance are the ray's geometrical characteristics at frequencies below the MUF. For this reason, we will next examine HFNET mode predictions with those of HFMUFES4 and data taken on the Slough to Cypress link.

Table 4 lists predicted values of mode type and elevation angle at frequencies between 6 MHz and 30 MHz at times of 2 and 10 hours (universal time) for HFMUFES4 and HFNET with two ionospheric models. HFNET was first run with its internal Aerospace ionospheric model. Then, the special HFNET version with the HFMUFES4 ionospheric model was used. This latter HFNET program was exercised in order to determine whether differences between HFNET and HFMUFES4 were due to the differing techniques of calculating mode geometry or due to the difference between the Aerospace and HFMUFES4 ionospheric models. By comparing HFMUFES4 and HFNET results obtained using the same ionospheric model, it was seen that essentially identical parameters (mode and elevation angle) were predicted. Further, the HFMUFES4 predicted value of MUF at UT - 2 is 17.54 MHz. In HFMUFES4, the MUF is defined as that frequency with a probability of 0.50. Thus, it would not be expected that HFNET, using the HFMUFES4 ionosphere, would predict a propagation mode at 18 MHz.

Comparison of columns 2 and 3 in Table 4 show that HFNET and HFMUFES4, with their individual ionospheric models, predict somewhat different propagation mode characteristics. At UT = 2, the HFNET predictions do not extend high enough in frequency due to the small value of f_oF_2 as described in the preceding discussion of MUF predictions. However, at frequencies for which propagation is predicted, there is good agreement between HFMUFES4 and HFNET modes and arrival angles. Note that in a case for which HFMUFES4 predicts a mode with probability less than about 0.5, HFNET does not generally calculate this mode. At UT = 10, when good agreement in MUF between HFNET and HFMUFES4 is obtained, good agreement between mode and elevation angle is also obtained. However, the HFNET elevation angles with the Aerospace model for one-hop F-layer propagation (at 22 MHz and 20 MHz) are consistently smaller by about 4°. Below 12 MHz, where propagation occurs via E modes, very close agreement in elevation angle is obtained. This would be expected by examination of Table 3 which shows that essentially identical E-layer characteristics are predicted by both models.

Table 4. Slough-Cypress propagation mode parameters, (a) UT = 2.

	HFMUFES4 (MUF = 17.54 MHz)			HFNET with Aerospace Model		HFNET with HFMUFES4 Model	
Frequency	Mode	Angle	Probability	Mode	Angle	Mode	Angle
20 MHz	1F	7.5	.10	-*	-	-	-
18	1F	7.5	.42	-	-	-	-
16	1F	5.0	.70	-	-	1F	4.9
14	1F	4.2	.87	-	-	1F	4.0
	2F	22.8	.04	-	-	-	-
12	1F	3.7	.94	1F	4.4	1F	3.5
	2F	22.8	.49	-	-	-	-
10	1F	3.4	.98	1F	2.0	1F	3.2
	2F	18.3	.83	-	-	2F	18.2
	3F	34.7	.29	-	-	-	-
8	1F	3.3	.99	1F	1.3	1F	3.0
	2F	17.1	.95	2F	16.2	2F	17.0
	3F	29.0	.80	-	-	3F	29.1
6	1F	3.6	.99	1F	1.5	1F	3.2
	2F	16.5	.99	2F	13.3	2F	16.3
	3F	27.0	.96	3F	26.0	3F	26.9

* A dash (-) indicates that HFNET does not predict a propagation mode at this frequency.

Table 4 (Continued). Slough-Cypress propagation parameters, (b) UT = 10.

	HFMUFES4 (MUF = 24.2 MHz)			HFNET with Aerospace Model		HFNET with HFMUFES4 MODEL	
Frequency	Mode	Angle	Probability	Mode	Angle	Mode	Angle
30 MHz	1F	7.1	.13	-*	-	-	-
28	1F	7.1	.22	-	-	-	-
26	1F	7.1	.36	-	-	-	-
24	1F	6.2	.51	-	-	1F	5.2
22	1F	4.4	.67	1F	0.25	1F	3.6
20	1F	4.1	.80	1F	0.08	1F	3.1
18	2F	20.5	.30	-	-	-	-
16	2F	18.7	.53	-	-	2F	17.3
	2E	3.9	.99	-	-	-	-
14	2F	16.0	.75	-	-	2F	14.6
	2E	3.5	.99	2E	0.24	-	-
12	2F	15.6	.91	-	-	3F	26.4
	2E	3.2	.99	2E	3.1	2E	3.4
10	3F	24.7	.84	-	-	3F	22.8
	2E	3.0	.99	2E	2.9	2E	3.3
	3E	7.5	.00	3E	7.3	3E	7.9
	2E	2.9	.47	2E	2.8	2E	3.1
	3E	7.2	.00	3E	7.1	3E	7.7
	2E	2.8	.00	2E	2.7	2E	3.0

* A dash (-) indicates that HFNET does not predict a propagation mode at this frequency.

Figure 4, from Reference 11, shows measured values of median angles of arrival via one- and two-hop F-layer modes for each month and four-hour period at frequencies of 9.9 MHz, 17.5 MHz, and 23.0 MHz. Comparison of this with the data in Table 4 can be made, although it must be kept in mind that Figure 4 contains yearly averaged data whereas Table 4 contains predicted values for the month of July. Table 5 lists values of yearly average data from Figure 4 and some HFMUFES4 and HFNET predictions. In general, there is a few degrees discrepancy between measured and predicted values of arrival angle.

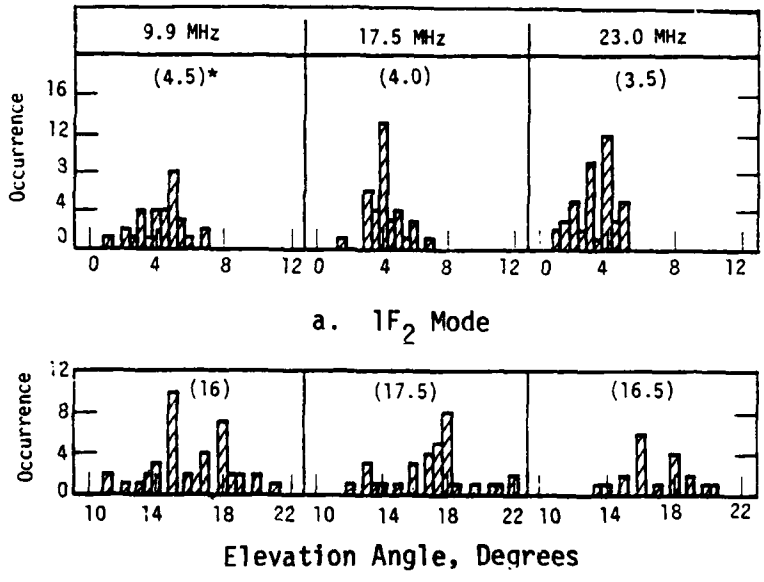

a. $1F_2$ Mode

b. $2F_2$ mode

* Values in brackets are overall medians for each mode and frequency.

Figure 4. Median Elevation angles.

It is interesting to note that both HFNET and HFMUFES4 predict a hole in propagation at UT = 10 hours; that is, propagation will not occur continuously between the MUF and the lowest operating frequency (LOF).

Table 5. Comparison of measured and predicted elevation angles for Slough to Cypress link.

(a) 1F Mode at 9.9 MHz

Measured Yearly Average	4.5°
10 MHz HFMUFES4 at UT = 2	3.4°
10 MHz HFNET at UT = 2	2.0°

(b) 1F Mode at 17.5 MHz

Measured Yearly Average	4.0°
18 MHz HFMUFES4 at UT = 2	7.5°
16 MHz HFMUFES4 at UT = 2	5.0°
No HFNET Mode	

(c) 1F Mode at 23 MHz

Measured Yearly Average	3.5°
22 MHz HFMUFES Mode at UT = 10	4.4°
22 MHz HFNET Mode at UT = 10	0.25°

(d) 2F Mode at 9.9 MHz

Measured Yearly Average	16.0°
10 MHz HFMUFES4 Mode at UT = 2	18.3°
No HFNET Mode	

(e) 2F Mode at 17.5 MHz

Measured Yearly Average	17.5°
18 MHz HFMUFES4 Mode at UT = 10	20.5°
No HFNET Mode	

Although the MUF is around 22 MHz to 24 MHz, HFNET predicts no propagation at 16 MHz or 18 MHz; the probability of the HFMUFES4 18 MHz 2F mode is 0.30.

We conclude that HFNET and HFMUFES4 algorithms for mode geometry are in good agreement, but that their respective F-layer ionospheric models may vary substantially. This variation in ionospheric models may give rise to large differences in mode characteristics, or existence, at higher frequencies. It was shown in Figure 1 that the Aerospace model gave better agreement with data at Arecibo, Puerto Rico than did the HFMUFES4 model. The poorer agreement of the Aerospace model with data at UT = 2 on the Slough to Cypress link is insufficient evidence for automatically considering this ionospheric model to be invalid. The need for further evaluation of ionospheric models will be discussed in Section 4.

3.2.2 Azimuthal Arrival Angle

It is of interest to compare HFNET predicted values of azimuthal arrival angles with measured values. Reference 12 discusses angle of arrival data during the sunrise period on an HF link from Houston, Texas to Urbana, Illinois. Beacons operating at 8 MHz and 12.2 MHz were monitored and angle of arrival (AoA) measurements were made during a year's time. In general, measured values of AoA deviation from great-circle arrival were of the order of 0.5° to 1.5°, values which are probably unimportant to the kind of problems to be studied using HFNET. A seasonal dependence was noted with smallest deviations measured during winter months. Of course, wide variability of daily measurements was evident—a ubiquitous characteristic of ionospheric measurements. HFNET values of deviation of arrival angle from the great-circle paths were of the order of 0.1° for June and 0.3° for March.

Thus, the HFNET predicted values of non-great-circle arrival angle for mid-latitudes are somewhat smaller than those observed, but the entire phenomenon is relatively unimportant at these latitudes. The reason for smaller HFNET values is undoubtedly due to the median-value nature of the ionospheric model; the Aerospace model (and all others) do not accurately represent the variability (spatial or temporal) of the real ionosphere.

3.3 RESULTS IN THE AURORAL REGION

3.3.1 Mode Characteristics

Much work has been done to understand HF propagation in the auroral region with application to communications and over-the-horizon (OTH) radar. Reference 13 summarizes measurements from Caribou, Maine to Keflavik, Iceland, Thule, and Narssarssuaq, Greenland. Figure 5 shows the geometrical relationship between the transmitter and receiver sites, and the auroral oval. This is truly auroral region propagation. Figures 6, 7, and 8 show measured and HFNET predicted values of MOF and LOF on these paths for November 1972. It should be noted that the measurements were limited to an upper limit of 26 MHz so that measured values of MOF at 26 MHz may not represent the true MOF. The measured MOF's and LOF's to the three receiver stations are averaged over between about three and eight days of observations depending upon the particular location. During the observation period, the ionosphere remained relatively quiet with the K_p index varying between 1^- and 3^-. The HFNET values were obtained with an assumed average value of $K_p = 2^-$. When HFNET was run with K_p values of 1 and 3, little change in MOF (of the order of 0.5 MHz) was noted. The RADC polar ionosphere model was used for these predictions.

The HFNET predicted LOF values were obtained in the following way, which is substantially different than that used to get the MOF.

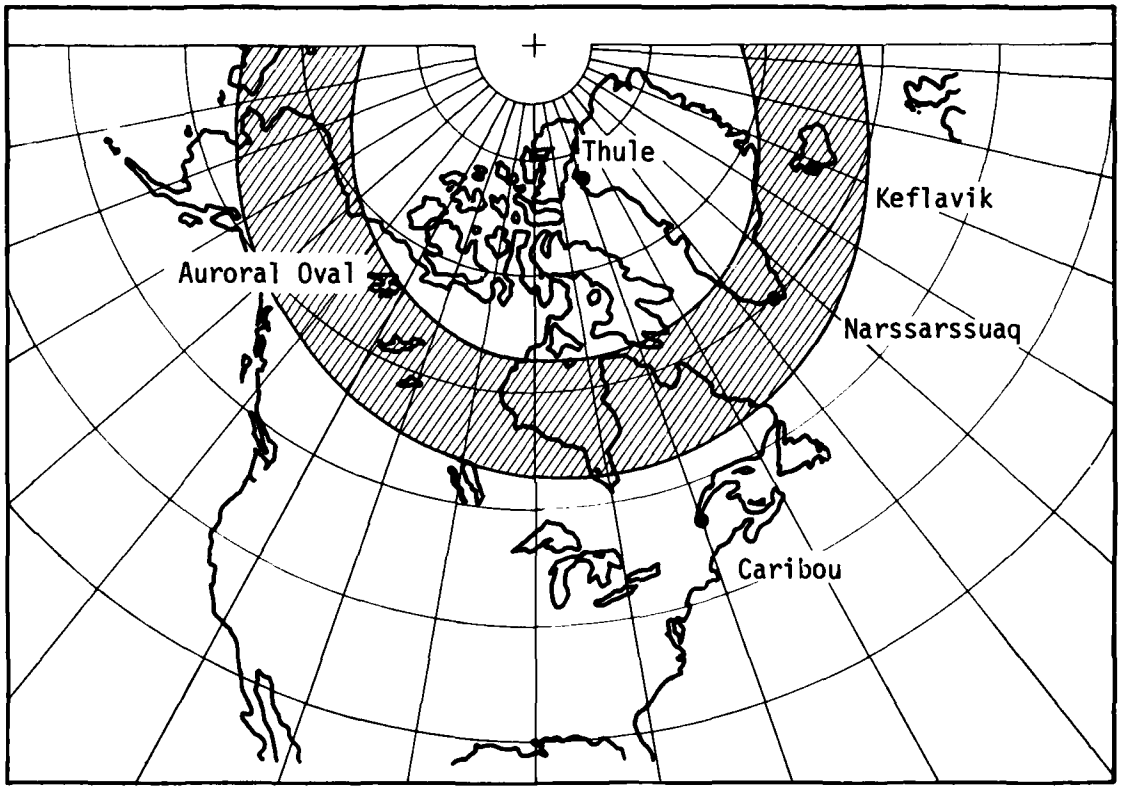

Figure 5. Geometry of auroral region propagation paths.

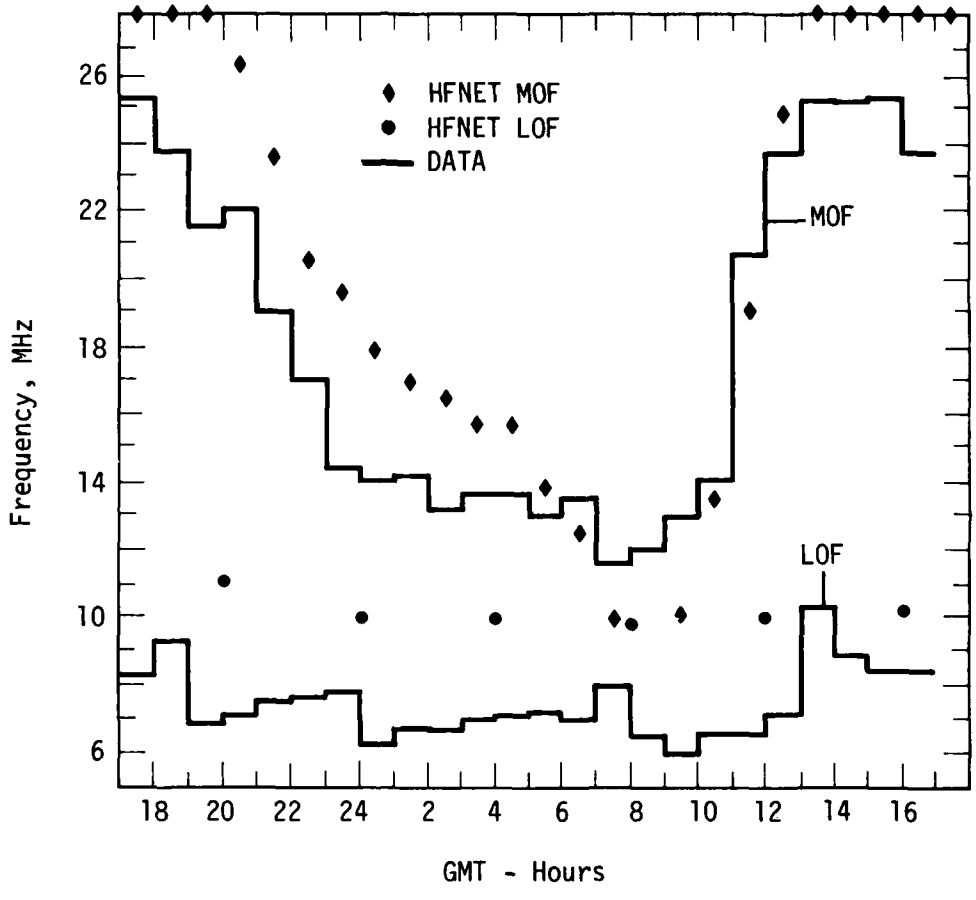

Figure 6. Predicted and measured MOF and LOF for Caribou-Keflavik path.

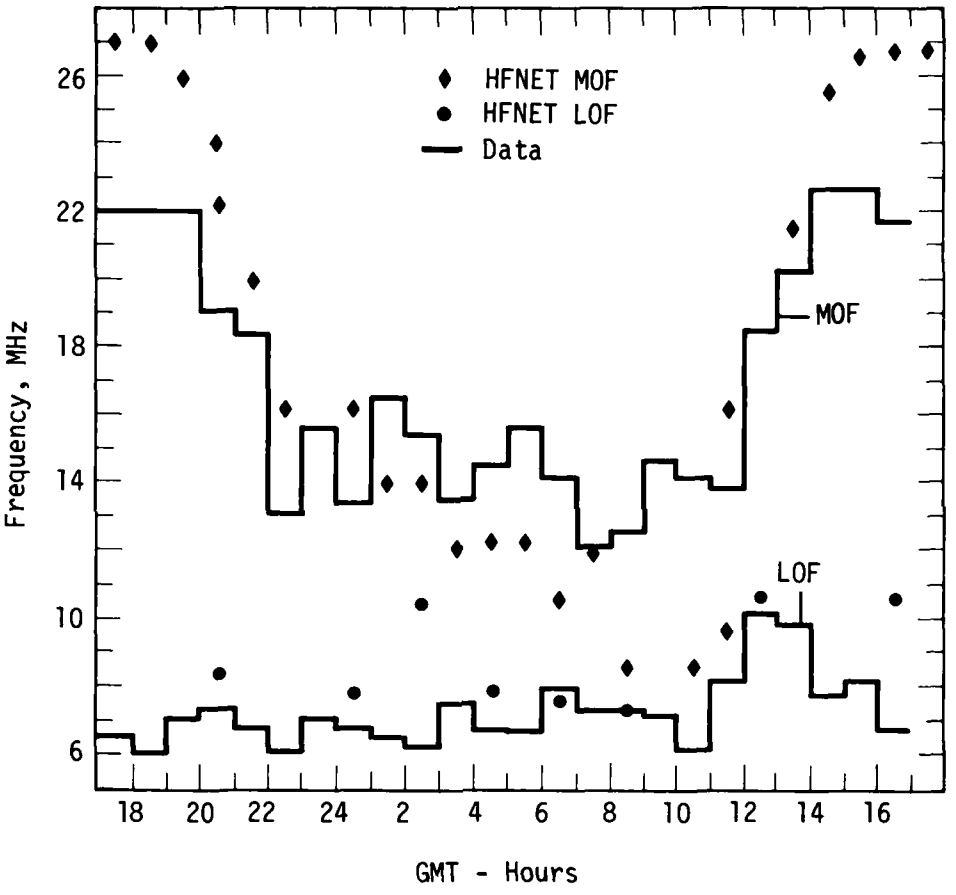

Figure 7. Predicted and measured MOF and LOF for Caribou-Narssarssuaq path.

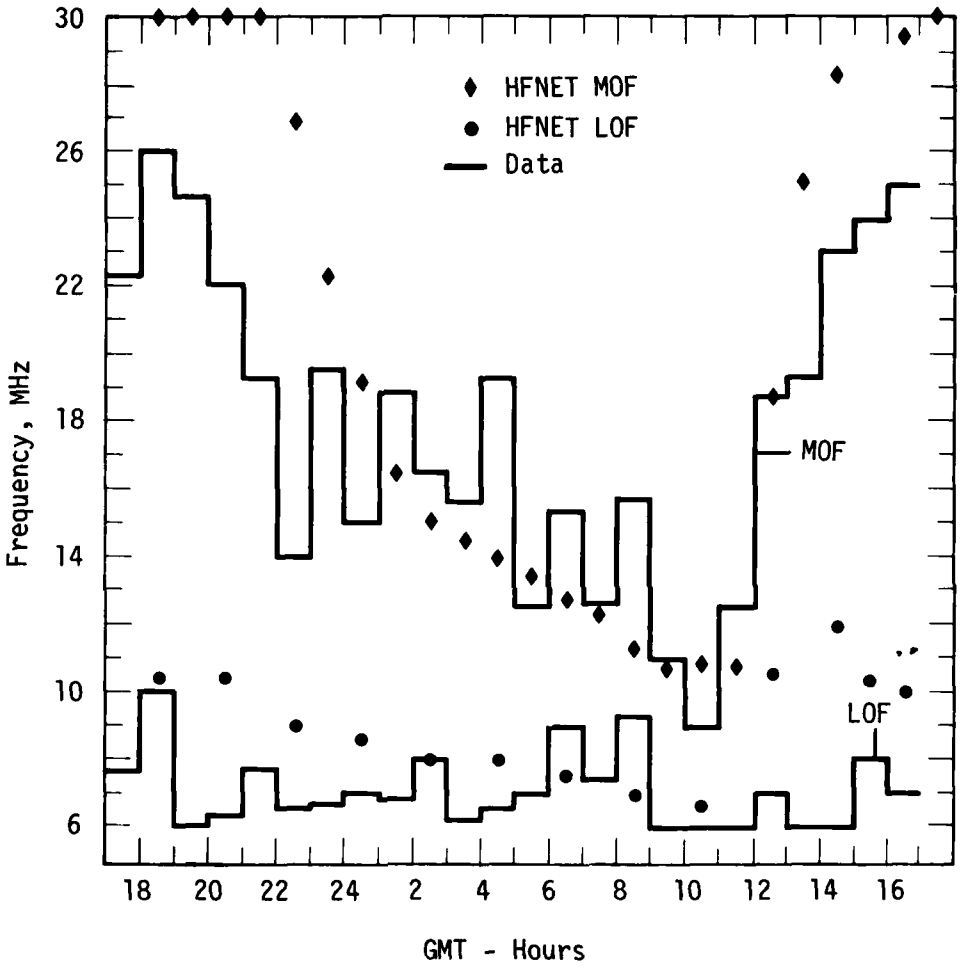

Figure 8. Predicted and measured MOF and LOF for Caribou-Thule path.

The MOF is determined by the F_2 critical frequency at the path midpoint. The LOF is less clearly defined since it is generally determined by the magnitude of D-region absorption along the entire path. The amount of D-region absorption which causes an HF link to "black out" depends upon the S/N ratio at the receiver and the receiver sensitivity. These parameters are unavailable to us so we make the following assumption. We assume that a particular value of D-region absorption is sufficient to produce link outage at the lower frequencies. In this case, the value of 10 dB has been used. Thus, HFNET mode and D-region absorption predictions are examined and the LOF is arbitrarily selected to be that frequency at which 10 dB of D-region absorption is produced. Note that if a higher value of absorption had been selected (i.e., 20 dB), a lower value of LOF is obtained.

A further comment about the predicted LOF values should be noted. The D-region absorption in the auroral region is controlled by magnetic storm characteristics. This is in contrast to mid- and equatorial-latitudes, where the absorption is controlled by insolation. It was mentioned earlier that the auroral region data shown in Figures 6, 7, and 8 were taken during a period in which the K_p value varied between 1^- and 3^-. While this variation in K_p produced an insignificant variation in predicted values of MOF (insignificant in the sense of the overall uncertainty in the entire HF link predictive capability), the D-region absorption varies dramatically with this change in K_p value. For example, Table 6 lists representative values of predicted D-region absorption for various K_p values for a mode between Caribou and Keflavik at 8 MHz. It is seen that a change in K_p value of two units produces a change of more than 10 dB in absorption (at 8 MHz on this link). The values of LOF were taken from HFNET predictions for a constant K_p value of 2, whereas the LOF data is averaged over varying K_p values.

Table 6. Dependence of predicted auroral D-region absorption on K_p index; 8 MHz link ($1F_2$) between Caribou and Keflavik.

K_p	Absorption (dB)
0	6.6
2	19.4
4	33.2
6	47.8
8	64.9

Predicted values of MOF on the Caribou-Narssarssuaq link were also obtained using the Aerospace ionosphere. Figure 9 shows measured MOF values and those predicted with the RADC and Aerospace ionosphere models. The Aerospace MOF values are substantially lower than those measured as was the case in the mid-latitude links examined in Section 3.2.1.

3.3.2 Azimuthal Arrival Angle

As part of a high latitude propagation experiment[14,15], azimuthal angle-of-arrival measurements and the amount of angular spreading were made for auroral propagation between an aircraft operating at a range of between 900 km and 3,000 km from a series of receiving antennas at Goose Bay, Labrador. Two-way oblique ionograms were measured at both ends of the path for frequencies between 6 MHz to 16 MHz. Complex data analysis techniques were used because of the aircraft motion during the time over which the oblique soundings were made. Most of the data consisted of E-layer modes because they occurred most of the time and because, when other modes were present, the E mode was generally the strongest. Although the median value for the absolute angular deviation was 2° from the true bearing to the aircraft, and well within the uncertainty of the aircraft position, maximum deviations of 9° were seen. The median value of the angular

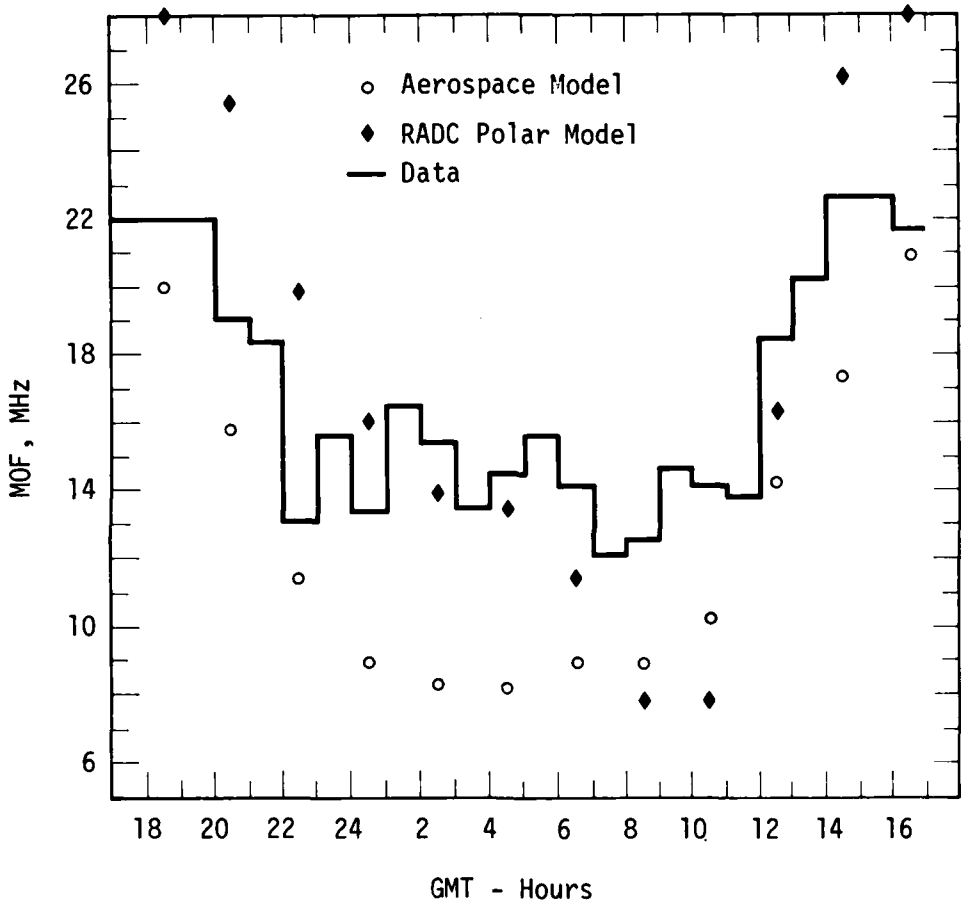

Figure 9. Dependence of ionospheric model on MOF predictions - Caribou-Narssarssuaq link.

spreading was 4°; it varied between 2° and 6° and was essentially the same value for E—or F—mode signals. They concluded that large arrival angles were caused by a tilted ionosphere. At many times, multiple modes with varying arrival angles were observed, and this is attributed to a traveling ionospheric wave. They also observed positive and negative deviations with equal overall probability but with different time dependencies. Prior to 2200 UT, 82 percent of the deviations were to the west, whereas after 2200 UT, 83 percent were to the east. Their explanation for this is that higher critical frequencies lie to the west of the path midpoint in the afternoon (before 2200 UT) as a result of effects of solar control. The gradient to the west, increasing from about 2.5 MHz at the midpoint to about 3 MHz some 700 km west, tends to make the arrival angle deviate to the west of the true path. After 2200 UT, the approaching auroral oval with a median nighttime critical frequency at 2 MHz to 3 MHz is thought to provide the mechanism for changing the gradient.

Calculations of predicted propagation characteristics were made using HFNET for paths from 1,000 km and 2,000 km north of Goose Bay to Goose Bay in order to compare predicted angles of arrival with the DAASM data. Four frequencies, at 13.2 MHz, 11.2 MHz, 8.2 MHz, and 6.2 MHz, were studied. In general, predicted angles of arrival were less than 0.2° from the great-circle direction; a few deviations approaching 1° were obtained. Thus, the predicted angles of arrival are substantially smaller than those observed. This is, undoubtedly, due to the lack of realistic non-uniformities in horizontal gradients obtained from the use of the median ionosphere.

SECTION 4
CONCLUSIONS

In the preceding sections, several types of comparisons have been made. HFNET results were compared with results from HFMUFES4 and with data representative of mid-latitude and auroral region propagation links. Within HFNET, two elements—the geometrical model of propagation and the ionospheric model—were shown to essentially determine the program output parameters.

In evaluating the ambient mode predictions of HFNET, it is necessary to keep in mind which predicted mode characteristics are most important. The ultimate purpose of HFNET is to study propagation in a nuclear burst environment. The effects of nuclear bursts on ambient modes are, for the most part, limited to excess D-region absorption. The characteristics of ambient mode predictions affecting predicted D-region absorption are the position of the D-region crossing with respect to the nuclear bursts and the path length through this region (related to the angle of passage through the D-region).

Thus, the geometrical parameters at frequencies of interest are of primary concern. Unfortunately, much of the data used for comparison with HFNET results is in the form of MUF. This parameter is of limited interest because most communications occur at frequencies substantially below the MUF. Furthermore, selection of MUF for comparison is unfortunate because of its sensitivity upon ionospheric characteristics which, as was seen, are highly variable. Thus, although MUF is a convenient parameter to measure and is most often used to summarize

propagation data, it is not of high importance (unless, of course, propagation occurs at or near this frequency).

Verification of HFNET's geometrical models was made by comparing its mode characteristics with data and also with those from HFMUFES4 for the case in which an identical ionospheric model was used in both computer programs. It was seen in Section 3.2.1 that essentially identical mode characteristics were predicted by both programs over the Slough to Cypress path when the HFMUFES4 ionospheric model was used. Furthermore, the computer code predictions agreed well with experimental observations.

It was seen that substantial variation occurs in the characteristics of the natural ionosphere and that this variability gives rise to variability in predicted and measured parameters of ionospheric propagation. Figure 2 showed daily variations in MUF of from 10 percent to 20 percent on the 3,200 km Slough to Cypress link. The magnitude of this measured daily variability of MUF is the same as that predicted using ray tracing techniques and measured variations in ionospheric parameters. Thus, Table 3 showed that changes on the order of 10 percent to 20 percent in MUF were produced by normal daily ionospheric variability.

For the case of mid-latitude propagation, it was seen in Section 3.2 that predicted values of mode characteristics changed somewhat when different ionospheric models were used. HFNET uses a fast running analytic model of global ionospheric characteristics which yields smaller values of F-layer critical frequency than the HFMUFES4 model for the Slough to Cypress link, with the result, shown in Figure 3, that HFNET values of MUF are between 5 percent and 20 percent smaller than those predicted by HFMUFES4. The HFNET values still fall within the measured daily variability of MUF.

For the case of auroral region propagation, HFNET uses the RADC polar ionosphere model, and in Section 3.3 it was seen that good agreement between predicted and measured values of MUF were obtained.

However, since most communication links operate below the MUF so as to avoid the daily ionospheric variations, the ability of a particular computer program to predict the MUF may not be important. Table 4 shows HFNET and HFMUFES4-predicted values of elevation angle of arrival for the Slouth to Cypress link, and it is seen that agreement to within a few degrees is generally obtained. Table 5, showing predicted and measured azimuthal arrival angles, illustrates that predicted values are generally within a few degrees of measured values.

HFNET contains models of non-great-circle propagation arising from horizontal gradients in the ionosphere. Comparison of predicted and measured azimuthal angles, for both mid-latitude and auroral regions, shows that predicted values are much smaller than measured values. The reason for smaller predicted deviations from great-circle paths is thought to be caused by the median nature of the ionospheric models. That is, the horizontal fluctuations in the ionospheric parameters, which give rise to the real but highly variable non-great-circle arrival angles, are essentially averaged out in the process of forming median models of the ionosphere. It should be noted, however, that the magnitude of the measured deviations from the great-circle are generally quite small—of the order of 2° to 5°.

REFERENCES

1. G. W. Haydon, et al., Predicting the Performance of High Frequency Sky-Wave Telecommunications Systems (The Use of the HFMUFES4 Program), OT Report 76-102, Office of Telecommunications, September 1976.

2. D. H. Sowle, An Ambient HF Radio Mode Model, DNA 4420T, Mission Research Corporation, September 1977.

3. B. K. Ching, and Y. T. Chiu, "A Phenomenological Model of Ionospheric Density," Journal of Atmospheric and Terrestrial Physics, 35, pp 1615, 1973.

4. Y. T. Chiu, "An Improved Phenomenological Model of Ionospheric Density," Journal of Atmospheric and Terrestrial Physics, 37 pp 1563, 1975.

5. T. J. Elkins, and C. M. Rush, "A Statistical Predictive Model of the Polar Ionosphere." In An Empirical Model of the Polar Ionosphere, AFCRL-TR-73-0331, Air Force Cambridge Research Laboratories, Bedford, Massachusetts, May 1973.

6. R. R. Vondrak, et al., Chatanika Model of the High-Latitude Ionosphere for Application to HF Propagation Prediction, RADC-TR-787, Stanford Research Institute, January 1978.

7. Gordon Rostocker, "Geomagnetic Indices," Reviews of Geophysics and Space Physics, 10, No. 4, pp 935-959, November 1972.

8. E. J. Fremouw, et al., A Transionospheric Communication Channel Model, Quarterly Technical Report 7, Stanford Research Institute, July 1977.

9. C. L. Rino, et al., Two Fortran Programs for Calculating Ionospheric Amplitude and Phase Scintillation, Quarterly Report 8, Stanford Research Institute, July 1977.

REFERENCES (Continued)

10. C. M. Rush, et al., "The Relative Daily Variability of f_0F_2 and h_mF_2 and Their Implications for HF Radio Propagation," Radio Science, 9, pp 747, August-September 1974.

11. P. A. Bradley, and D. R. Howard, "Transmission Loss at High Frequencies on 3,260 km Temperate Latitude Path," Proceedings of IEE, 120, pp 173, February 1973.

12. N. N. Rao, and R. I. Beckwith, "Prediction of Azimuth Angle of Arrival of HF Waves During the Sunrise Period," Radio Science, 9, pp 617, June 1974.

13. Propagation data from the Raytheon Company's Polar Fox II experimental program was made available by Charles Callahan of the MITRE Corporation, Bedford, Massachusetts.

14. G. S. Sales, et al., DAASM Project - High Latitude Aircraft HF Propagation Report, *AFCRL-TR-0290*, Air Force Cambridge Research Laboratories, Bedford, Massachusetts, May 1975.

15. G. S. Sales, and J. I. Videberg, DAASM - High Latitude Aircraft HF Propagation Experiment, Part II, TR-76-235, Rome Air Development Center, Bedford, Massachusetts, July 1976.

APPENDIX

In June, 1978 and at DNA's direction, a version of HFNET was delivered to Science Applications, Incorporated (SAI), La Jolla, California for their use in studies supporting the Air Force Studies and Analysis Group. That version did not contain the most accurate nuclear burst effects since the inclusion of such effects into HFNET was under vigorous development at that time. The fact that the June, 1978 version of HFNET was soon to be superseded by a significantly improved program was recognized by DNA, MRC, and SAI. While the newer versions of HFNET include the auroral ionosphere, improved nuclear burst phenomenology, and bomb modes, the earlier version contains the Aerospace ionosphere model and ambient mode geometry model described in this report. This appendix contains a few additional comparisons between HFNET and HFMUFES4 for hypothetical links from Omaha to points 2,000 km and 4,000 km east of Omaha.

Figures A-1 and A-2 show predicted values of MUF from the two programs for conditions in March and a sunspot number of 120. It is seen that HFNET values are somewhat smaller than HFMUFES4 as was seen in section 3.2.1. As was described earlier, comparison of predicted values of MUF is a convenience. In terms of predicting nuclear burst effects on links operating at frequencies below the MUF, which is the objective of HFNET, the geometric relationship between the D-region crossing point and the location of the fission debris region is the major factor determining nuclear burst effects. The similarity between arrival angles

predicted with the two programs, indicating essentially identical mode geometries, was demonstrated in section 3.2.1 and is also true for these cases.

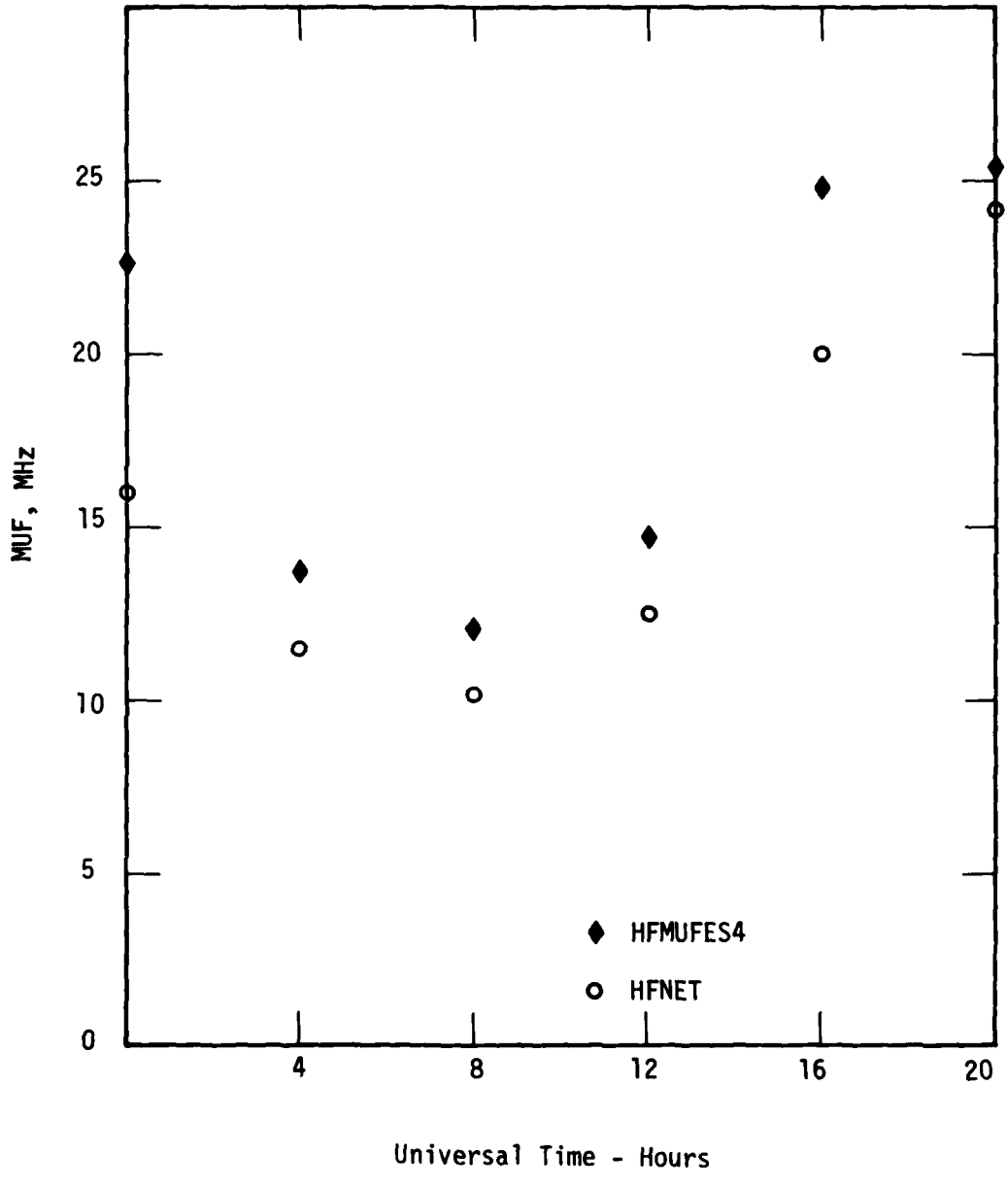

Figure A-1. Predicted values of MUF for a hypothetical 2,000 km path.

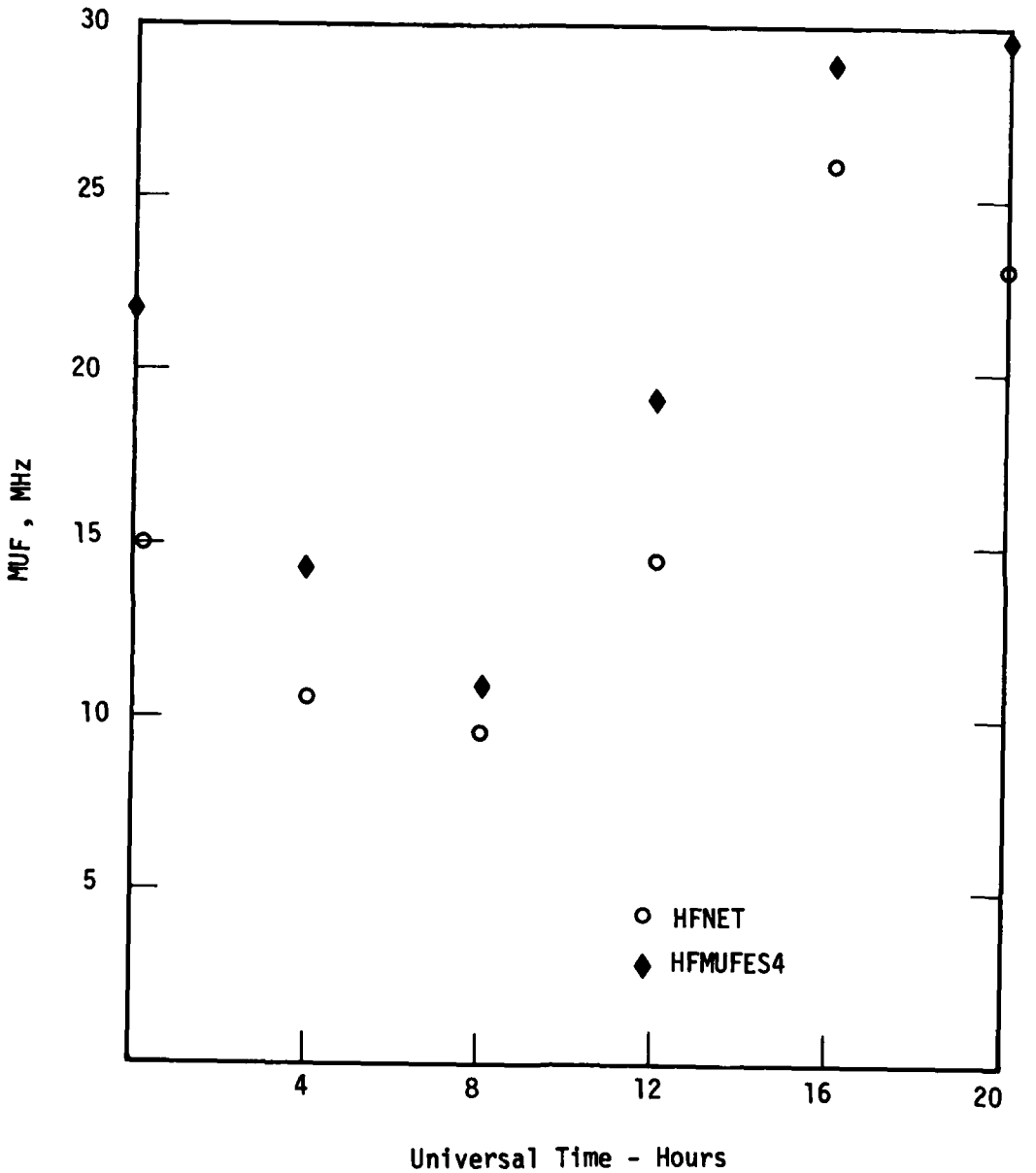

Figure A-2. Predicted values of MUF for a hypothetical 4,000 km path.

DISTRIBUTION LIST

DEPARTMENT OF DEFENSE

Assistant Secretary of Defense
Comm., Cmd., Cont. & Intell.
ATTN: Dir. of Intelligence Systems, J. Babcock
ATTN: C3IST&CCS, M. Epstein

Assistant to the Secretary of Defense
Atomic Energy
ATTN: Executive Assistant

Command & Control Technical Center
ATTN: C-650, G. Jones
ATTN: C-312, R. Mason
3 cy ATTN: C-650, W. Heidig

Defense Advanced Rsch. Proj. Agency
ATTN: TIO

Defense Communications Agency
ATTN: Code R1033, M. Raffensperger
ATTN: Code 101B
ATTN: Code 205
ATTN: Code 480
ATTN: Code 810, J. Barna

Defense Communications Engineer Center
ATTN: Code R123
ATTN: Code R410, J. McLean
ATTN: Code R720, J. Worthington

Defense Intelligence Agency
ATTN: HQ-TR, J. Stewart
ATTN: DB-4C, E. O'Farrell
ATTN: DC-7D, W. Wittig
ATTN: DB, A. Wise
ATTN: DT-5
ATTN: DT-1B

Defense Nuclear Agency
ATTN: STVL
ATTN: DDST
3 cy ATTN: RAAE
4 cy ATTN: TITL

Defense Technical Information Center
12 cy ATTN: DD

Field Command
Defense Nuclear Agency
ATTN: FCPR

Field Command
Defense Nuclear Agency
Livermore Division
ATTN: FCPRL

Interservice Nuclear Weapons School
ATTN: TTV

Joint Chiefs of Staff
ATTN: C3S
ATTN: J-37
ATTN: J-3, WWMCCS Evaluation Office

Joint Strat. Tgt. Planning Staff
ATTN: JLTW-2
ATTN: JPST, G. Goetz

DEPARTMENT OF DEFENSE (Continued)

National Security Agency
ATTN: B-3, F. Leonard
ATTN: W-32, O. Bartlett
ATTN: R-52, J. Skillman

Undersecretary of Defense for Rsch. & Engrg.
ATTN: Strategic & Space Systems (OS)

WWMCCS System Engineering Org.
ATTN: R. Crawford

DEPARTMENT OF THE ARMY

Assistant Chief of Staff for Automation & Comm.
Department of the Army
ATTN: DAAC-ZT, P. Kenny

Atmospheric Sciences Laboratory
U.S. Army Electronics R&D Command
ATTN: DELAS-EC, F. Niles

BMD Systems Command
Department of the Army
2 cy ATTN: BMDSC-HW

Deputy Chief of Staff for Ops. & Plans
Department of the Army
ATTN: DAMO-RQC

Electronics Tech. & Devices Lab.
U.S. Army Electronics R&D Command
ATTN: DELET-ER, H. Bomke

Harry Diamond Laboratories
Department of the Army
ATTN: DELHD-N-P
ATTN: DELHD-N-RB, R. Williams
ATTN: DELHD-I-TL, M. Weiner
ATTN: DELHD-N-P, F. Wimenitz

U.S. Army Comm.-Elec. Engrg. Instal. Agency
ATTN: CCC-EMEO, W. Nair
ATTN: CCC-CED-CCO, W. Neuendorf
ATTN: CCC-EMEO-PED, G. Lane

U.S. Army Communications Command
ATTN: CC-OPS-W
ATTN: CC-OPS-WR, H. Wilson

U.S. Army Communications R&D Command
ATTN: DRDCO-COM-RY, W. Kesselman

U.S. Army Foreign Science & Tech. Ctr.
ATTN: DRXST-SD

U.S. Army Materiel Dev. & Readiness Cmd.
ATTN: DRCLDC, J. Bender

U.S. Army Nuclear & Chemical Agency
ATTN: Library

U.S. Army Satellite Comm. Agency
ATTN: Document Control

DEPARTMENT OF THE ARMY (Continued)

U.S. Army TRADOC Systems Analysis Activity
ATTN: ATAA-TCC, F. Payan, Jr.
ATTN: ATAA-PL
ATTN: ATAA-TDC

DEPARTMENT OF THE NAVY

Joint Cruise Missile Project Office
Department of the Navy
ATTN: JCM-G-70

Naval Air Development Center
ATTN: Code 6091, M. Setz

Naval Air Systems Command
ATTN: PMA 271

Naval Electronic Systems Command
ATTN: PME 106-13, T. Griffin
ATTN: PME 117-20
ATTN: PME 106-4, S. Kearney
ATTN: PME 117-211, B. Kruger
ATTN: Code 501A
ATTN: Code 3101, T. Hughes
ATTN: PME 117-2013, G. Burnhart

Naval Intelligence Support Ctr.
ATTN: NISC-50

Naval Ocean Systems Center
ATTN: Code 5322, M. Paulson
ATTN: Code 532, J. Bickel
ATTN: Code 8151, C. Baggett
3 cy ATTN: Code 5324, W. Moler

Naval Research Laboratory
ATTN: Code 7550, J. Davis
ATTN: Code 7500, B. Wald
ATTN: Code 6700, T. Coffey
ATTN: Code 6780, S. Ossakow
ATTN: Code 7555
ATTN: Code 7580

Naval Space Surveillance System
ATTN: J. Burton

Naval Surface Weapons Center
ATTN: Code F31

Naval Surface Weapons Center
ATTN: Code F-14, R. Butler

Naval Telecommunications Command
ATTN: Code 341

Office of Naval Research
ATTN: Code 421
ATTN: Code 420

Office of the Chief of Naval Operations
ATTN: OP 604C
ATTN: OP 981N
ATTN: OP 941D

Strategic Systems Project Office
Department of the Navy
ATTN: NSP-43
ATTN: NSP-2722, F. Wimberly
ATTN: NSP-2141

DEPARTMENT OF THE AIR FORCE

Aerospace Defense Command
Department of the Air Force
ATTN: XP
ATTN: XPDQ

Aerospace Defense Command
Department of the Air Force
ATTN: DC, T. Long

Air Force Avionics Laboratory
ATTN: AAD, W. Hunt
ATTN: AAD, A. Johnson

Air Force Geophysics Laboratory
ATTN: OPR-1, J. Ulwick
ATTN: PHI, J. Buchau
ATTN: LKB, K. Champion
ATTN: PHP, J. Aarons
ATTN: OPR, A. Stair
ATTN: PHP, J. Mullen

Air Force Weapons Laboratory, AFSC
ATTN: DYC
ATTN: SUL

Air Logistics Command
Department of the Air Force
ATTN: OO-ALC/MM, R. Blackburn

Assistant Chief of Staff
Intelligence
Department of the Air Force
ATTN: INED

Assistant Chief of Staff
Studies & Analyses
Department of the Air Force
ATTN: AF/SASC, W. Adams
ATTN: AF/SASC, G. Zank

Ballistic Missile Office
Air Force Systems Command
ATTN: MNNL, S. Kennedy
ATTN: MNNH

Deputy Chief of Staff
Operations Plans and Readiness
Department of the Air Force
ATTN: AFXOXFD
ATTN: AFXOKCD
ATTN: AFXOKT
ATTN: AFXOKS

Deputy Chief of Staff
Research, Development, & Acq.
Department of the Air Force
ATTN: AFRDQ
ATTN: AFRDS
ATTN: AFRDSS
ATTN: AFRDSP

Electronic Systems Division
Department of the Air Force
ATTN: DCKC, J. Clark

Electronic Systems Division
Department of the Air Force
ATTN: XRW, J. Deas

DEPARTMENT OF THE AIR FORCE (Continued)

Electronic Systems Division
Department of the Air Force
ATTN: YSM, J. Kobelski
ATTN: YSEA

Foreign Technology Division
Air Force Systems Command
ATTN: SDEC, A. Oakes
ATTN: TQTD, B. Ballard
ATTN: NIIS Library

Headquarters Space Division
Air Force Systems Command
ATTN: SKA, C. Rightmyer
ATTN: SKA, M. Clavin

Headquarters Space Division
Air Force Systems Command
ATTN: SZJ, L. Doan

Rome Air Development Center
Air Force Systems Command
ATTN: TSLD
ATTN: OCS, V. Coyne

Rome Air Development Center
Air Force Systems Command
ATTN: EEP

Strategic Air Command
Department of the Air Force
ATTN: DCXT, T. Jorgensen
ATTN: XPFS
ATTN: DCX
ATTN: OOKSN
ATTN: DCXT
ATTN: DCXF
ATTN: NRT

DEPARTMENT OF ENERGY CONTRACTORS

Lawrence Livermore Laboratory
ATTN: Document Control for Technical Information Dept. Library

Los Alamos Scientific Laboratory
ATTN: Document Control for P. Keaton
ATTN: Document Control for D. Westervelt
ATTN: Document Control for R. Taschek

Sandia Laboratories
ATTN: Document Control for D. Thornbrough
ATTN: Document Control for 3141
ATTN: Document Control for Org. 1250, W. Brown
ATTN: Document Control for D. Dahlgren
ATTN: Document Control for Space Project Div.

Sandia Laboratories
Livermore Laboratory
ATTN: Document Control for B. Murphy
ATTN: Document Control for T. Cook

EG&G, Inc.
ATTN: Document Control for D. Wright
ATTN: Document Control for J. Colvin

OTHER GOVERNMENT AGENCIES

Central Intelligence Agency
ATTN: OSI/PSTD

Department of Commerce
National Bureau of Standards
ATTN: Security Officer for R. Moore

Department of Commerce
National Oceanic & Atmospheric Admin.
Environmental Research Laboratories
ATTN: R. Grubb

Institute for Telecommunications Sciences
National Telecommunications & Info. Admin.
ATTN: L. Berry
ATTN: W. Utlaut
ATTN: A. Jean
ATTN: D. Crombie

U.S. Coast Guard
Department of Transportation
ATTN: G-DOE-3/TP54, B. Romine

DEPARTMENT OF DEFENSE CONTRACTORS

Aerospace Corp.
ATTN: D. Olsen
ATTN: T. Salmi
ATTN: F. Morse
ATTN: I. Garfunkel
ATTN: N. Stockwell
ATTN: S. Bower
ATTN: V. Josephson
ATTN: R. Slaughter

University of Alaska
ATTN: N. Brown
ATTN: Technical Library
ATTN: T. Davis

Analytical Systems Engineering Corp.
ATTN: Radio Sciences

Analytical Systems Engineering Corp.
ATTN: Security

Barry Research Communications
ATTN: J. McLaughlin

BDM Corp.
ATTN: T. Neighbors
ATTN: L. Jacobs

Berkeley Research Associates, Inc.
ATTN: J. Workman

Boeing Co.
ATTN: G. Hall
ATTN: J. Kenney
ATTN: D. Murray
ATTN: S. Tashird

University of California at San Diego
ATTN: H. Booker

DEPARTMENT OF DEFENSE CONTRACTORS (Continued)

Charles Stark Draper Lab., Inc.
ATTN: D. Cox
ATTN: J. Gilmore

Computer Sciences Corp.
ATTN: H. Blank

Comsat Labs.
ATTN: G. Hyde
ATTN: R. Taur

Cornell University
ATTN: D. Farley, Jr.

Electrospace Systems, Inc.
ATTN: H. Logston

ESL, Inc.
ATTN: J. Roberts
ATTN: J. Marshall
ATTN: C. Prettie

Ford Aerospace & Communications Corp.
ATTN: J. Mattingley

General Electric Co.
ATTN: M. Bortner

General Electric Co.
ATTN: C. Zierdt
ATTN: S. Lipson
ATTN: A. Steinmayer

General Electric Co.
ATTN: F. Reibert

General Electric Company-TEMPO
ATTN: M. Stanton
ATTN: DASIAC
ATTN: T. Stevens
ATTN: D. Chandler
ATTN: W. Knapp

General Electric Tech. Services Co., Inc.
ATTN: G. Millman

General Research Corp.
ATTN: J. Ise, Jr.
ATTN: J. Garbarino

GTE Sylvania, Inc.
ATTN: M. Cross

HSS, Inc.
ATTN: D. Hansen

IBM Corp.
ATTN: F. Ricci

University of Illinois
ATTN: Security Supervisor for K. Yeh

Institute for Defense Analyses
ATTN: J. Bengston
ATTN: H. Wolfhard
ATTN: E. Bauer
ATTN: J. Aein

DEPARTMENT OF DEFENSE CONTRACTORS (Continued)

International Tel. & Telegraph Corp.
ATTN: Technical Library
ATTN: G. Wetmore

JAYCOR
ATTN: S. Goldman

JAYCOR
ATTN: D. Carlos

Johns Hopkins University
ATTN: J. Newland
ATTN: B. Wise
ATTN: T. Evans
ATTN: P. Komiske
ATTN: T. Potemra
ATTN: Document Librarian

Kaman Sciences Corp.
ATTN: T. Meagher

Linkabit Corp.
ATTN: I. Jacobs

Litton Systems, Inc.
ATTN: R. Grasty

Lockheed Missiles & Space Co., Inc.
ATTN: R. Johnson
ATTN: M. Walt
ATTN: W. Imhof

Lockheed Missiles & Space Co., Inc.
ATTN: Dept 60-12
ATTN: D. Churchill

M.I.T. Lincoln Lab.
ATTN: D. Towle
ATTN: L. Loughlin

McDonnell Douglas Corp.
ATTN: J. Moule
ATTN: W. Olson
ATTN: G. Mroz
ATTN: N. Harris

Mission Research Corp.
ATTN: D. Sowle
ATTN: R. Hendrick
ATTN: F. Fajen
ATTN: R. Bogusch
ATTN: M. Scheike
6 cy ATTN: S. Gutsche
6 cy ATTN: W. Schleuter
5 cy ATTN: Document Control

Mitre Corp.
ATTN: G. Harding
ATTN: A. Kymmel
ATTN: C. Callahan

Mitre Corp.
ATTN: M. Horrocks
ATTN: W. Hall
ATTN: W. Foster

Pacific-Sierra Research Corp.
ATTN: E. Field, Jr.

DEPARTMENT OF DEFENSE CONTRACTORS (Continued)

Pennsylvania State University
ATTN: Ionospheric Research Lab.

Photometrics, Inc.
ATTN: I. Kofsky

Physical Dynamics, Inc.
ATTN: E. Fremouw

R&D Associates
ATTN: C. MacDonald
ATTN: R. Turco
ATTN: F. Gilmore
ATTN: W. Wright, Jr.
ATTN: W. Karzas
ATTN: R. Lelevier
ATTN: M. Gantsweg
ATTN: C. Greifinger
ATTN: B. Gabbard
ATTN: H. Ory

R&D Associates
ATTN: L. Delaney

Rand Corp.
ATTN: C. Crain
ATTN: E. Bedrozian

Riverside Research Institute
ATTN: V. Trapani

Rockwell International Corp.
ATTN: J. Kristof

Santa Fe Corp.
ATTN: E. Ortlieb

Science Applications, Inc.
ATTN: D. Divis

DEPARTMENT OF DEFENSE CONTRACTORS (Continued)

Science Applications, Inc.
ATTN: J. McDougall
ATTN: E. Straker
ATTN: D. Hamlin
ATTN: D. Sachs
ATTN: C. Smith
ATTN: L. Linson

Science Applications, Inc.
ATTN: SZ

SRI International
ATTN: A. Burns
ATTN: G. Smith
ATTN: G. Price
ATTN: R. Livingston
ATTN: D. Neilson
ATTN: M. Baron
ATTN: R. Leadabrand
ATTN: C. Rino
ATTN: W. Chesnut
ATTN: W. Jaye

Teledyne Brown Engineering
ATTN: R. Deliberis

Tri-Com, Inc.
ATTN: D. Murray

TRW Defense & Space Sys. Group
ATTN: D. Dee
ATTN: R. Plebuch
ATTN: S. Altschuler

Utah State University
ATTN: L. Jensen
ATTN: K. Baker

Visidyne, Inc.
ATTN: J. Carpenter